THE PENNSYLVANIA STATE UNIVERSITY
SCHREYER HONORS COLLEGE

DEPARTMENT OF BIOMEDICAL ENGINEERING

DEVELOPMENT OF A NOVEL MAGNESIUM DOPED CITRATE BASED POLYMER COMPOSITE FOR ORTHOPEDIC ENGINEERING

KEVIN MICHAEL RAHN
SPRING 2018

A thesis
submitted in partial fulfillment
of the requirements
for a baccalaureate degree
in Biomedical Engineering
with honors in Biomedical Engineering

Reviewed and approved* by the following:

Jian Yang
Professor of Biomedical Engineering
Thesis Supervisor, Honors Advisor

Justin Brown
Professor of Biomedical Engineering
Faculty Reader

Keefe Manning
Professor of Biomedical Engineering
Schreyer Honors College Associate Dean for Academic Affairs
Thesis Committee Member

* Signatures are on file in the Schreyer Honors College.

ABSTRACT

Current bone substitute materials vary greatly both in their manufacturing techniques and compositions, but many still lack the mechanical, biological, and fabrication properties for a clinically ready bone substitute material. The goal of this study was to develop a novel self-setting polymer/ceramic composite bone cement with improved manufacturability through the use of a citrate polymer, a calcium phosphate mineral phase, and magnesium oxide as a self-setting agent. Magnesium oxide (MgO) was shown to quickly self-set POC (poly (octamethylene citrate)) polymer and POC/hydroxyapatite (HA) composites suitable as bone tissue substitute materials. A predictive model for the setting time of the cement as a function of cement composition was developed, as well as a preliminary setting reaction mechanism model for the cement. The mechanical properties of the cement, including the peak stress, Young's modulus, and peak strain were characterized and shown in cases of lower MgO concentrations to significantly improve the peak stress and Young's modulus of the material. Additionally, the cytotoxicity, degradation, pH response, and swelling response of the material were shown to be either comparable, or an improvement on POC/HA control composites. Finally, and most notably, the increased ease of fabrication of porous and solid scaffolds through injection molding was demonstrated, providing a drastic improvement on current routes of fabrication for POC/HA composites. The applicability of magnesium oxide self-setting was also demonstrated in other polymers of the citrate polymer family, including crosslinked urethane doped polyester elastomers (CUPE), biodegradable photoluminescent polymer (BPLP), and POC-click.

TABLE OF CONTENTS

LIST OF FIGURES

LIST OF TABLES

ACKNOWLEDGEMENTS

I would like to thank Ethan Gerhard, Dr. Jinshan Guo, and Dr. Jian Yang for their guidance and friendship during my three years in the Transformative Biomaterials and Biotechnology lab. Each of you played an important role in my development both as a person and as a researcher; thank you. I'd also like to thank Dr. Justin Brown and Dr. Keefe Manning for their advice and suggestions during the thesis writing process. Finally, I'd like to thank my mom and dad, Chris and Jeanne, for being wonderful parents and for their willingness to listen to my problems and offer advice.

Chapter 1

Introduction

1.1 Challenges in Bone Tissue Engineering

Although the engineering of biomaterials for the regeneration of bone tissue in the body has seen significant improvement both in terms of process and material development since the first clinical applications of biomaterials in orthopedic cases, there still exists a need for the development of new bone substitute materials. The gold standard for bone substitutes, autologous bone graft, has inherent issues with donor site morbidity and limited supply [1]. In developing new biomaterials for these orthopedic applications, several important characteristics must be considered; orthopedic biomaterials, although a broad group of materials with varied applications, should all be compatible with natural bone tissue in the body. Materials should not trigger aggressive immune response and degradation products should have low cytotoxicity. Additionally, orthopedic biomaterials should mimic the natural mechanical properties of the tissue which they are replacing or attempting to regenerate; for bone this necessitates a material with high compressive strength and Young's Modulus. Finally, a major consideration for orthopedic biomaterials is the route of manufacture by which the material can be fabricated; techniques ranging from porogen leaching, to 3D printing, to solvent casting all offer unique advantages and disadvantages depending on the application. Designing a material which can easily be fabricated in a range of geometries is a major step away from the small-scale production of academic research and towards the clinical applications of industrial scale manufacturing.

The development of biomaterials which offer all of these characteristics has proven a massive challenge. Some materials may offer significant biological activity yet lack the mechanical properties required as a cell bearing scaffold or implantable material. Others may be ideal mechanically, yet be

biologically incompatible, produce toxic degradation products, or lack the ability to drive cell growth and differentiation into the desired tissue type. Even materials which may seem viable for a tissue regeneration application in almost all ways may have difficulties in the manufacture or fabrication techniques used to produce the material. The challenge of tissue engineering is not only understanding the intricacies of cell differentiation, tissue growth, scaffold material properties, and fabrication techniques, but balancing all of these considerations into a material, fabrication technique, and tissue growth strategy which addresses all of these concerns adequately.

1.2 Early Self-Setting Bone Substitute Materials

In general, the properties of any biomaterial are driven by its eventual clinical application. The unique physiological and pathological characteristics of certain areas of orthopedic surgery, most notably craniofacial surgery, drives the need for versatile biomaterials capable of self-setting and moldability, but also of high enough mechanical strength to prevent failure. Plaster of Paris, a gypsum plaster ($CaSO_4 \cdot 2H_2O$), is one of the earliest examples of an in situ self-setting material used in orthopedic surgeries to fill both small and large voids in bone; although plaster requires heating to about 300ºC to begin hardening, it's moldability and lack of an immune response gave an early solution to reconstruction of large bone defects [2]. In contrast to calcium sulfate plaster, calcium phosphate (CaP) materials were also used as bone substitutes as early as 1920, with tricalcium phosphate ($Ca_3(PO_4)_2$, TCP) being implanted *in vivo* to replace lost osseous tissue. Variation of calcium to phosphate molar ratios and crystalline structure gave rise to a variety of CaP materials, yet almost all of these materials required high temperature sintering to form implantable bone substitutes, limiting the use of these materials in truly self-setting, *in situ* applications. Attempts at a self-setting inorganic bone substitute in the vein of single calcium phosphate formulations generally failed as a result of either the need for prolonged high temperature, or a massive change in pH which precludes *in situ* use. Additionally, sintered ceramic

calcium phosphate materials presented the disadvantage of inability to be reabsorbed by the body; essentially a fused block, these ceramics did not allow for the true regeneration of natural tissue.

A major breakthrough in the development of a self-setting bone substitute came with the development of the first calcium phosphate cement (CPC) by Brown and Chow in 1985; a near saturated mix of $Ca_4 (PO_4)_2O$ (tetracalcium phosphate) and one of several other calcium phosphate particles at equilibrium was shown to precipitate hydroxyapatite (HA, $Ca_5(PO_4)_3(OH)$) without the need for extended high temperature or a harmful change in pH [3]. In addition to being truly self-setting at a physiological pH, these CPCs also saw an advantage in their ability to be reabsorbed by the body; a precipitated calcium phosphate lacked the fused morphology of a sintered ceramic, allowing a breakdown of the material over time. Despite the improvement on early ceramic bone substitutes, CPCs still lacked the ability to truly drive tissue regeneration; reabsorption of the material was shown to be very slow [4], and in general, the material was far from reaching the "gold standard" of bone substitute materials in that of autologous bone with respect to bioactivity and mechanical properties. Additionally, CPCs showed low mechanical strength, limiting their applications to largely craniofacial regions [5].

1.3 Recent Developments in Self-Setting Bone Substitute Materials

Since the development of CPCs in the early days of tissue engineering, a better understanding of the complexity of tissue regeneration has driven research into more functional, bioactive, and versatile materials. What began as simple calcium phosphate cements has now developed into multi-component ceramic/polymer composites [6-10], modified cements capable of drug delivery and cell encapsulation [11-13], and silicate, bio-glass, or other inorganic additive doped CPCs with varied properties [14-18]. Despite the vast research into these materials, there still remain unsolved issues with bone substitute materials.

1.4 Increased Ease of Scaffold Manufacture by Injection Molding and 3D Printing

Fabrication techniques can often be an overlooked aspect of biomaterial design. Often the efficiency of fabrication will be neglected to further improve mechanical or biological properties, and this limits the applications of the material as it is translated from academic research to clinical applications and industrial scale manufacture. As a result, there is remarkably little research on the injection molding of orthopedic biomaterials. Injection molding is a materials processing technique with massive importance in the polymer and plastic industries [19]. By compressing a flowable polymer above its glass transition temperature (T_g) into a three-dimensional mold, a solid polymer shape can be obtained with high tolerances and relatively easy processing. The injection molding technique for plastics has been heavily studied, but in general, the technique has been rarely used with tissue engineered polymers and composites. Although in many cases bioactive polymers provide good compatibility and mechanical properties for tissue engineering applications, these polymers can also degrade at much lower temperatures, often below the temperature required for injection molding. Although sub varieties of injection molding such as reaction injection molding (RIM) provide different mechanisms for the curing step of the injection molding process, and limited success has been seen with injection molded PEEK/HA composites [20], PLA/PVOH polymer blends [21], and starch-based degradable scaffolds [22], in general the use of injection molding has been limited in the biomaterials field.

Wu et al. (2006) describe the challenges of injection molding temperature sensitive polymers with tissue engineering objectives in mind; firstly, a major challenge of porous tissue engineering scaffolds is reaching a high porosity and interconnected pore structure, while still maintaining desired mechanical properties and ease of manufacture [23]. With respect to injection molding, this challenge remains difficult to overcome; incorporating a leachable particulate such as salt into the material can decrease the flowability of the material to such a degree that injection molding is impossible. Wu et al. (2006) developed a "wet" method for injection molding PCL and PLGA which relied on adding a solvent phase to the material to increase its flowability, thus allowing high levels of porosity (>90%) to be routinely

reached. Again, however, this technique was not without flaws; when solvent fractions reached higher levels, although the flowability and ease of injection molding were increased, the scaffold would not maintain its shape after being removed from the mold. Additionally, due to the evaporation of the solvent after the molding process, scaffolds saw some shrinkage, although described as uniform and able to be controlled in the process [23]. Despite these challenges, the room temperature injection molding technique offers some advantages to the more traditional solvent casting, or compression molding techniques routinely used for porous scaffold fabrication.

Additive manufacturing/3D printing, like injection molding, relies on a material's ability to harden or set within a period of time. Generally, these techniques are used with thermoplastic materials which can be melted during the printing/molding process, and which then cool and solidify. Although some thermoplastic polymers used as biomaterials (PLA, PLGA) can be printed via this route, many other biocompatible polymers are thermoset polymers, preventing a straightforward 3D printing of the material.

Some research has examined the "wet" printing or setting of materials; this approach uses a dual phase method of a solid and solvent phase, usually with some form of binder solution to set the material during the printing or setting process. Inzana et al. (2014) illustrated the ability to print calcium phosphate/collagen composite scaffolds with a phosphoric acid binding solution, but higher concentrations of the binder solution showed significantly increased cytotoxicity [24]. Cytotoxicity of binder solutions limits the mechanical properties of the printed material, as higher concentrations of binder generally increase strength, but are often toxic to cells and therefore unusable. Although scaffolds were printed with phosphoric acid concentrations low enough to limit cytotoxicity, the mechanical properties of these scaffolds were limited, with low compressive yield strengths and porosities. Cox et al. (2015) used poly(vinyl)alcohol (PVA) in combination with HA as a viscous printable material, but these composites too showed low compressive strength and poor osteoconductivity [25].

Other techniques focus on the modification of approved calcium phosphate cements for printing purposes. Lode et al. (2014) developed a water-based setting technique for on the market CPCs by

incorporating a triglyceride, Polysorbate 80, and phosphoric acid into a binding solution which was then able to set in contact with water in 5-8 minutes. The self-setting paste was flowable enough to 3D print simple scaffold geometries with strand size of 838um for the modified CPC, however supporting PVA was required to maintain the shape of the construct as the paste hardened. In addition to this fabrication limitation, the printed scaffolds saw a low compressive yield strength (2.5MPa), and a reduced number of viable cells on the printed scaffold material compared to an unmodified calcium phosphate cement of the same inorganic formulation. The authors suggested that this decreased cytocompatibility was due to the prolonged setting time in which the setting reaction may have continued to occur during cell culture, slightly modifying the pH and Ca^{2+} concentration of the culture medium [26].

3D printing offers a unique approach to scaffold manufacture, both from a fabrication aspect, and from the increased flexibility and detail of scaffolds which may influence tissue growth. Although there are certainly benefits of an additive manufacturing approach, it seems clear that current 3D printed materials face serious problems, especially for bone regeneration applications. Almost all 3D printed bone scaffolds simply lack the mechanical properties desired of a bone substitute material, and those that come close do so at the cost of cytocompatibility by incorporating additional setting components. In the case of these materials, an ideal self-setting mechanism is one in which the additive adds to the cytocompatibility and osteoinductive abilities of the material.

Although there remain unsolved problems for translating injection molding and 3D printing to the tissue engineering and regenerative medicine field, the benefits of developing new techniques and/or materials capable of these techniques offers attractive routes of fabrication. Much of the research done in tissue engineering requires delicate, hands on manufacturing techniques; solvent casting and compressive molding, although relatively simple for researchers to do in small amounts, are difficult to use on the industrial scale. As research moves forward towards addressing clinical issues and away from the lab, materials which are easily manufactured, with high accuracy and processability will be superior to materials without these industrially required characteristics. Injection molding has been shown to be a

highly competitive manufacturing technique, indicating its potential for the scaling up of tissue regenerative materials.

1.5 Citrate-based Materials: A Promising Area for Orthopedic Material Design

Citrate-based materials offer a unique approach to the issues faced in several areas of biomaterial design such as soft tissue engineering, neural engineering, and bioimaging, but they also have notable applications as orthopedic biomaterials [27]. Citrate, or citric acid, is a common organic molecule found in the body as a byproduct of the Krebs Cycle, or Citric Acid Cycle. Dual carboxylic acid groups allow for simple polymerization via a polycondensation reaction with diol monomers which results in a degradable ester bond and "pendant" geometry (Fig. 1) for functionalization of the polymer [28]. Although the family of citrate based polymers has grown since its first development, the elastomer poly(octamethylene citrate) (POC) remains the most studied of these polymers [29]. Degradation products of citric acid and 1-8 octanediol limit cytotoxicity, and elastomeric properties lend POC to applications in drug delivery, vascular and soft tissue engineering [27]. The fabrication of a polymer/ceramic composite with POC and hydroxyapatite (HA) has shown promise as an orthopedic material; citrate's role in bone growth and apatite formation has been well documented [30], and the polymer's ability to form interactions with HA in a composite improves the mechanical properties of the material [31].

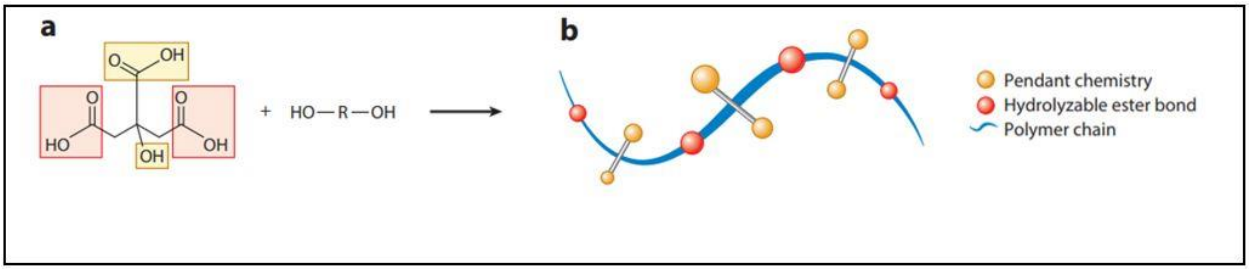

Figure 1: General composition of citrate based materials (Reused with permission from Tran et al. 2015, [29]). Citric acid reacts with a diol via a polycondensation reaction to form a polymer with hydrolysable ester bonds and carboxylic pedant geometry via citrate.

Although citrate-based polymers show promise in orthopedic biomaterial applications, these polymer and polymer/ceramic composites show some limitations in the form of the processability of the materials, slower degradation rate, and slightly acidic pH response. As with most thermoset polymers, POC can be solvent cast to form films, as well as salt leached to form porous scaffolds [27]. However, the polymer's inability to set quickly without high concentrations of nonbiocompatible chemical crosslinkers or prolonged high temperature crosslinking limits it's use as an injectable, 3D printable, or injection moldable material. With a renewed interest in additive manufacturing techniques, and the improved ease of manufacturability of injection molding, there exists a need for a new manufacturing technique for these citrate-based polymers. A nontoxic, biocompatible material, capable of setting citrate-based polymers/composites would allow for the expansion of this class of materials into the additive manufacturing and injection molding areas, as well as improve the current solvent casting/salt leaching techniques.

1.6 Magnesium Based Materials and their Role in Orthopedic Engineering

Metal alloys were some of the earliest orthopedic materials, with stainless steel used as early as the 1920s and alloys of titanium still in use for certain applications today [32]. The exploration of other metals for biomedical applications has opened a new area of orthopedic materials; recently, metals such as magnesium, strontium, and cobalt based alloys have gained interest. Of these, magnesium is unique in its similarity of mechanical properties to that of natural bone; magnesium metal is softer than other orthopedic metals, with a Young's modulus, density, and compressive yield strength within the range of natural bone [33].

Additionally, magnesium plays a vital role both in a general biological sense, as well as specifically in bone tissue. Magnesium acts as a cofactor for several enzymes and as a stabilizing ion for DNA and RNA. Over half of all magnesium in the body is stored in bone, and magnesium has been

shown to have a significant impact on the rate of bone tissue growth; Zrieqat et al. (2002) showed that alumina disks implanted with magnesium ions showed increased cell attachment for human bone-derived cells [34]. Yamasaki (2002) similarly illustrated an increased adhesion of osteoblast cells on functionally graded carbonate apatite containing magnesium, as well as the promotion of bone formation in collagen-carbonate apatite containing magnesium composites [35,36]. An *in vivo* study of magnesium alloy implants in a guinea pig femur model by Witte et al. (2005) further confirmed the potential for bone tissue stimulation by magnesium; magnesium containing alloy implants showed a significant increase in mineralized bone area after 8 and 16 weeks when compared to a PLA control group. Magnesium alloy groups also showed no evidence of cytotoxicity, further indicating its potential as an orthopedic implant material. Although magnesium alloys show promise as an implant material, several studies have shown potential setbacks for these materials in the form of gas formation during the degradation of the implant; although Witte et al (2005) claim no adverse effects were observed from gas bubble formation surrounding the implant, puncturing of the gas bubbles with a needle was still required, indicating a limitation of the magnesium-based alloys [37].

Other forms of magnesium have also shown promise in areas of biomaterial design, without the potential setbacks seen with metal alloys. Magnesium oxide (MgO) has been shown to improve the mechanics and biocompatibility of sintered HA/TCP materials. Tan et al. (2013) sintered MgO into HA at small percentages (0.05wt% - 1wt%) and determined that doping pure nanocrystalline HA with MgO showed a small increase in the Young's Modulus of the material and little cytotoxicity [38]. Banerjee et al. (2010) also found that MgO and SrO doped TCP increased cell growth and attachment to the material. Additionally, in a rat model, MgO doped TCP sintered implants (1% MgO) showed a better rate of bone growth via type I collagen and osteocalcin assays [39].

Magnesium has also been used as an additive in novel bone cements due to its acceleration of setting time, improved mechanical properties, and biological activity with respect to bone tissue. Jia et al. (2010) created a self-setting magnesium phosphate-based cement by combining 2:1 molar ratios of

magnesium oxide and calcium dihydrogen phosphate. The formation of magnesium phosphate and calcium phosphate via an acid base neutralization precipitated a solidified cement with a compressive strength of 43 MPa after 1 hour setting and 74 MPa after 7 days setting. The magnesium phosphate cement also showed a significant increase of both cell proliferation and ALP activity when compared to a tetra-calcium phosphate/dicalcium phosphate anhydrous cement control group, indicating it's potential for stimulating bone regrowth and osseointegration [40]. Li et al. (2013) used a similar magnesium calcium phosphate cement to fabricate porous scaffolds for *in vivo* implantation and found that the magnesium scaffolds showed a high percent interconnected pore structure (up to 80%), as well as full tissue integration 6 months post implantation in a rabbit femur model [41].

Research into the potential of magnesium as an additive to self-setting bone cements has seen expansion beyond traditional calcium-phosphate formulations. Recent research has examined the effects of magnesium in tricalcium-silicate cements, chitosan /HA composites, and phytic acid chelated magnesium phosphate cements. Liu et al. (2014) reported the novel combination of tricalcium silicate and magnesium phosphate into a self-setting cement with improved mechanical properties versus silicate or magnesium phosphate cements alone. A combination of these two cement types showed a compressive strength of 86 MPa, as well as stimulation of osteoblast cells and steady magnesium release [42]. Zima et al. (2017) examined the rheology and setting times of various magnesium doped hydroxyapatite/chitosan composites and found that the presence of magnesium ions, either freely in the composite, or sintered with hydroxyapatite prior to composite formation, disturbed the setting process by competing with calcium ions and actually slowed the setting times of the cement from 16 minutes to 54 minutes [43]. A noticeable change in the viscosity of the cement also indicated the chemical interaction of magnesium ions in the cement with chitosan; this finding was supported by Krajewska (2001) who found that magnesium ions showed low levels of affinity for chitosan gels [44]. Another recent example of magnesium bridging ceramic and organic components of a cement was Christel et al. (2015) who used phytic acid as a chelating agent in magnesium phosphate cements; although this same general principle

had been demonstrated by Konishi et al. (2013) with tricalcium phosphate and inositol phosphate, the ability of magnesium to similarly chelate phytic acid illustrates a relatively unexplored area of biomaterial development. These results indicate a potential for magnesium as a setting mechanism not just in pure ceramic cements, but also as a potential chelating agent in polymer/ceramic self-setting composites [45,46].

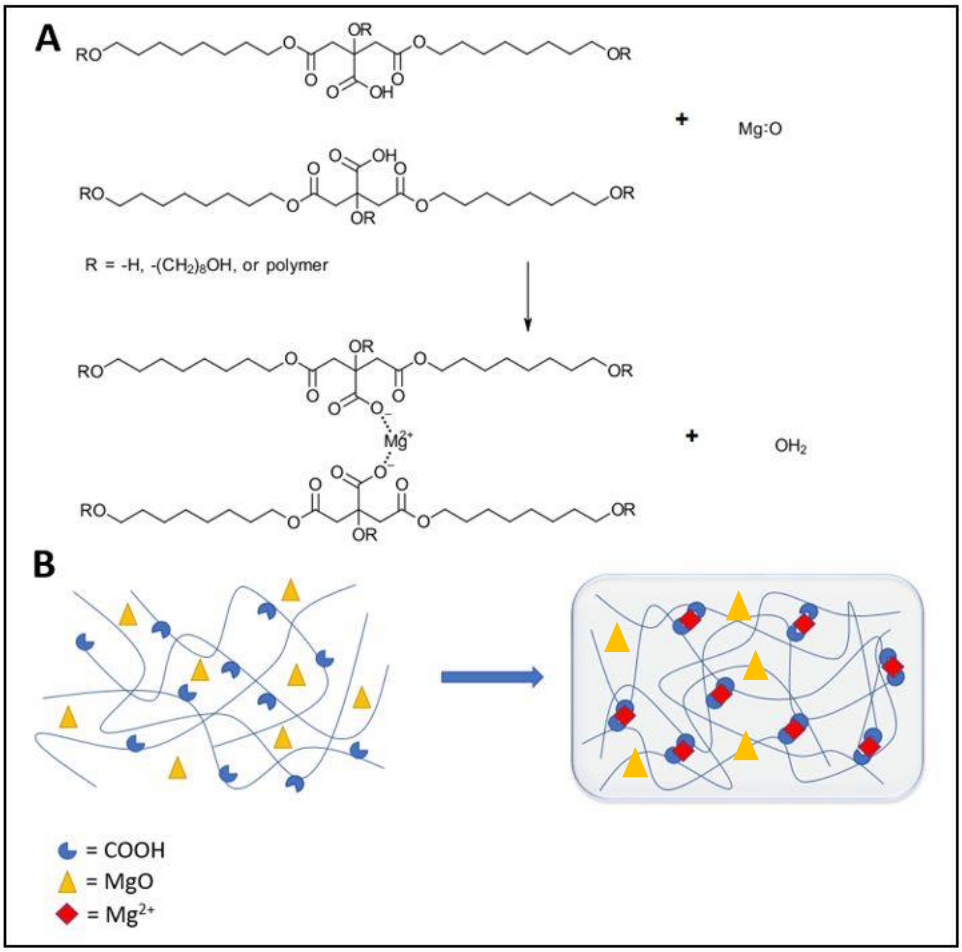

Figure 2: Expected chemical crosslinking mechanism of magnesium oxide in citrate polymers. Carboxylic acid pendant geometry provides reactivity for magnesium cation crosslinking, allowing for a chemical setting of citrate polymer without the need for extended thermal crosslinking.

1.7 The Novelty of a Self-Setting Citrate-based Composite for Bone Regeneration

In this thesis, we propose that magnesium oxide can act as a curing agent for citrate polymers, resulting in self-setting materials with improved mechanical and biological properties, diverse fabrication techniques, and applications to multiple areas of biomaterial research. Poly(octamethylene citrate) (POC), was chosen as the polymer component for polymer/ceramic composites due to its demonstrated potential as a bone regenerating polymer, biocompatibility, and previous use in a polymer/HA composite (Qiu et al., 2006). Previous scaffold fabrication techniques for POC have relied on either solvent casting of films, or compression molding of POC/HA scaffolds (R. Tran et al., 2009). Through the efficient self-setting ability of MgO in POC/HA composites, a material capable of both injection molding and 3D printing was developed. In addition to an increased ease of fabrication through these techniques, the magnesium induced self-setting of the material indicates a potential for a similar setting mechanism in other citrate-based materials. Evaluation of biological and physical properties of the novel material indicated a strong fit for the material in orthopedic applications.

Several specific aims were developed in response to current obstacles in self-setting bone materials for the novel material developed in this project. First, developing a predictive model for the setting time of the cement as a function of cement composition through exploratory factor analysis was desired. Fabrication techniques remain a major limitation of current scaffold materials. By developing a model capable of predicting the setting time of numerous multi-factor compositions of a POC-MgO material, future 3D printing or injection molding applications of the material will have a basic model from which to determine setting times. This aim was completed by determining the setting times of various POC-MgO compositions (varied polymer concentrations, monomer ratios, MgO concentrations, temperatures), and performing a factor analysis on the data to determine latent factors.

In addition to characterizing the setting mechanism, the mechanical properties of the material were desired to compare the material to previous POC/HA composites and natural bone tissue. Through ASTM standard compression testing of both thermally crosslinked and MgO crosslinked composites, the

yield strength, Young's modulus, and peak strain were determined. Additionally, the final material composition of MgO doped composites was determined through FTIR spectroscopy.

The third aim for this project was to characterize the biological activity of POC-MgO/HA materials. Cytotoxicity was evaluated by a CCK-8 cell proliferation assay of MgO doped POC/HA films, and pH, swelling, and degradation of the material was evaluated and compared to POC/HA controls. Additionally, the improved flexibility in processing was illustrated through basic scaffold fabrication via injection molding. An ideal cement composition was determined from the setting time model, and simple scaffolds and complex geometries were created. Manual 3D printing of MgO doped materials was also demonstrated as a proof of concept for later 3D printing attempts.

Finally, the applicability of the MgO setting in other citrate polymers was demonstrated; MgO was shown to self-set BPLP, CUPE, and POC-click polymers, as well as maintain these polymer's unique features, including fluorescence in the case of BPLP. Additionally, MgO doped POC was shown to have fluorescence, an interesting effect which should be explored further in the future.

Thesis Aims:

I. *Characterize the factors in setting time of MgO doped POC and develop a predictive factor analysis model for setting time*
II. *Evaluate the mechanical properties of MgO doped POC/HA composites*
III. *Characterize the biological and physical properties of MgO doped POC/HA*
IV. *Demonstrate novel routes of fabrication for MgO doped POC/HA*
V. *Evaluate the applicability of MgO doping in other citrate-based polymers and areas of biomaterial research*

Chapter 2

Materials and Methods

2.1 Pre-Polymer Synthesis and Purification

All chemicals were purchased from Sigma-Aldrich and used without further purification unless otherwise noted. The polymer component of all composites in this experiment was poly(octamethylene citrate) (POC) which was synthesized as described by our previous work (Yang et al., 2004). Briefly, predetermined molar ratios of citric acid and 1,8-octanediol (Table 1) were melted at 160^{o}C for 10 minutes. Temperature was then lowered to 140^{o}C and the flask was left to react until the stir speed was reduced to 60 rpm (approximately 1 hour). Once the stir bar was unable to stir at 60 rpm, the reaction was removed from heat and dioxane was added to stop the reaction. The pre-polymer solution was stirred vigorously overnight after being capped to prevent solvent loss.

Pre-polymer in dioxane was added dropwise to distilled water and stirred until the pre-polymer had formed a homogenous chunk around the stir rod. The distilled water was decanted and refilled and the solution was again stirred. After decanting a final time, the pre-polymer solution was frozen at –80^{o}C and lyophilized for 24 hours. The purified pre-polymer was then dissolved in ethanol at predetermined concentrations (30 wt%, 40 wt%, 50 wt%). POC of different citric acid:octanediol ratios was synthesized by the same method but according to the ratios in Table 1.

Table 1: POC synthesis molar ratios

	Amount for 1 batch of polymer			
[CA:OD]	Citric acid (mol)	1,8 octanediol (mol)	Citric acid (g)	1,8 octanediol (g)
1:1	0.1	0.1	19.21	14.62
1.1:1	0.11	0.1	21.13	14.62
1.3:1	0.13	0.1	24.98	14.62
1:1.1	0.1	0.11	19.21	16.08
1:1.3	0.1	0.13	19.21	19.01

2.2 Setting Time Determination

Magnesium oxide (MgO) was ground to <50µm using a sieve. MgO was dispersed in ethanol at 20% w/v and ultrasonicated for 10 minutes before use. To test the relative self-setting time, 1g of pre-polymer-MgO solution in ethanol was mixed in a 15mL centrifuge tube at predetermined ratios and set at the temperatures 25 ºC, 37ºC, and 75ºC (n=5). Samples were deemed to have set when tilting the tube at a 45-degree angle and tapping the tube for 30 seconds resulted in no change in the shape of the material.

2.3 Factor Analysis of Setting Time

The data analysis program Design-Ease (Stat-Ease Inc., Minneapolis) was used to develop a factor analysis model of the interactions of the factors on the setting time of the material. Pre-polymer concentration (30wt%, 40wt%, 50wt%), MgO concentration (5wt%, 10wt%, 15wt%), pre-polymer monomer molar ratio (1:1, 1:1.1, 1:1.3, 1.1:1, 1.3:1 [citric acid:octanediol]), and temperature (25ºC, 37ºC, 75ºC) were all factors which were experimentally shown to have an effect on the setting time of the material via analysis of variance (ANOVA). The setting time data for a fraction of the total combinations of these factors was collected and input under these four factors and effect plots, ANOVA, interaction

plots, and residual analysis were examined to determine a model that best fit the data. Model verification was performed on random combinations to confirm the accuracy of the predicted setting times.

2.4 Ceramic/Polymer Composite Fabrication

Composites of the POC pre-polymer, hydroxyapatite (HA), and MgO as the setting agent were fabricated and the material properties and setting times were determined. HA was added to the material at 15, 25, 35, 45, 50, and 55 wt% by mixing HA and MgO dry powders at the predetermined ratios and vigorously mixing with the pre-polymer. Setting time was determined as described above.

2.5 Mechanical Property Characterization

Cylindrical samples were fabricated for the determination of the Young's Modulus, maximum stress, and strain of the material after self-setting at room temperature. The self-setting polymer/HA/MgO composites were created at predetermined ratios (Table 2). The self-setting material was mixed as per the protocol for the self-setting test and loaded into a cylindrical syringe (inner diameter 5mm, 0.5 g composite per tube). The syringe was then capped and compressed to create a cylinder of length 10mm. Samples were then allowed to set in the syringe for 1 hr, 24 hr, or 72 hr. After this setting period, the cylinders were removed from the syringe and the remaining solvent was allowed to evaporate for 24 hours. Cylinders were then tested on an Instron 5966 machine fitted with a 10 N load cell (Instron, Norwood, MA) by applying a uniaxial compressive load. Young's Modulus was determined by the slope of the stress-strain curve from 0-10% elongation. 8 samples were performed for each composite formulation and setting time to determine the setting time dependence of mechanical properties of the material.

Table 2: Formula for 5g of POC-MgO/HA composites

Formulation	wt% POC	wt% MgO	wt% HA	POC (g)	MgO (g)	HA (g)
POC-MgO(5)HA(55)	40	5	55	2	0.25	2.75
POC-MgO(2.5)HA(57.5)	40	2.5	57.5	2	0.125	2.875
POC-MgO(1)HA(59)	40	1	59	2	0.05	2.95
POC-MgO(5)HA(45)	50	5	45	2.5	0.25	2.25
POC-MgO(2.5)HA(47.5)	50	2.5	47.5	2.5	0.125	2.375
POC-MgO(1)HA(49)	50	1	49	2.5	0.05	2.45

The mechanical properties of thermally crosslinked cylinders were determined by following the above procedure until removal of the sample from the syringe, at which point samples were thermally crosslinked at one of two predetermined crosslinking conditions (3d 80ºC, or 3d 80ºC + 3d 120ºC under vacuum). Cylinders were tested on an Instron 5966 machine fitted with a 10 N load cell (Instron, Norwood, MA) by applying a uniaxial compressive load. Young's Modulus was determined by the slope of the stress-strain curve from 0-10% elongation. 8 samples were performed for each composite formulation and setting time to determine the setting time dependence of mechanical properties of the material.

2.6 Bioactivity Characterization

Cytotoxicity of POC/HA/MgO films (n=8) was assessed against 3T3 cells using established protocols based on ISO standard. Briefly, 96 well plate composite disks were leached in DMEM supplemented with 10% FBS and 1% antibiotic solution with media change every 24 hours until no color change was observed (indicating neutral pH and leaching of the acidic sol content of the composites) then placed in a 96 well plate. 3T3 cells were seeded at a density of 5,000 cells/well with 200uL DMEM/well. PLGA and tissue culture plate served as positive and negative control, respectively. Samples were stored

in an incubator at 37C and 5% CO_2 for 24 hours, after which CCK-8 cytotoxicity assay was performed via the manufacturer's instructions and the samples were incubated for 2 hours (DMEM with CCK-8 solution was used as a background control for imaging). DMEM/CCK-8 solutions were removed and placed in a clean 96 well plate, and absorbance was measured at 450nm using a microplate reader. Background absorbance was subtracted and absorbance was normalized to tissue culture plate control.

2.7 Injection Molding of Composites

Bone 3D mold geometries were designed using the image processing software MIMICS, CAD software SolidWorks, and 3D printed using an Ultimaker 2 printer. Using a CT scan of the skull, a 3D geometry of the temporomandibular joint and coronoid process was extracted and processed in Solidworks. Injection molding molds were printed using an Ultimaker 2 printer with PLA (200um layer height) and a Formslab Form 2 SLA desktop printer (50um layer height). A POC-MgO/HA composite of 2.5wt% MgO and 47.5wt% HA was used for all injection molding. The wet composite was mixed at room temperature and injected into the 3D printed mold by hand. After in-mold setting at room temperature for 24 hours, the composite was removed from the mold and dried at room temperature for 2 days. After determining the optimal pressure and setting times for injection molding a solid composite, porous scaffolds were fabricated by particulate leaching the injection molded composites with NaCl (100-250 um, 60% porosity).

2.8 Physical Characterization via FTIR

The physical composition of MgO doped materials was determined by FTIR spectroscopy (Fourier-Transform Infrared Spectroscopy). HA, magnesium citrate tribasic, and MgO particles were used as standards to compare with POC-MgO and POC-MgO/HA composites.

2.9 Mineralization

10mm diameter disks were crosslinked at 3d 80^{o}C, 3d 120^{o}C vacuum and fixed to the bottom of a deep Teflon dish with vacuum grease. The samples were submerged in 5X SBF (simulated body fluid) at 37^{o}C. SBF solution was changed every other day. Samples were removed at time points (1d, 3d, 7d), lyophilized, and imaged with SEM at 500X magnification.

2.10 Degradation Study

The degradation profile of magnesium doped composites was determined using an accelerated degradation study. 7mm diameter, 1mm thick disks of POC/HA, POC-MgO/HA 1/49, POC-MgO/HA 2.5/47.5, and POC-MgO/HA 5/45 (n=8, crosslinked at 3d 80^{o}C, 3d 120^{o}C vacuum) were weighed and placed in 10 mL 0.02 M NaOH solution and incubated on an orbital shaker at 37^{o}C. At time points of 12 hr, 1d, 3d, 7d, 10d, and 14d, the NaOH solution was removed and the disks were rinsed with DI water and lyophilized for 5 days. Disks were then reweighed and the percent weight remaining was calculated according to Equation 1.

Equation 1:

$$\% \text{ Weight Remaining} = [(\text{Final Sample weight})/(\text{Initial Sample Weight})] \times 100$$

2.11 pH Study

The effect of magnesium oxide doping on the pH of the composite was tested and compared to POC/HA controls. 7mm diameter, 1mm thick disks of POC/HA, POC-MgO/HA 1/49, POC-MgO/HA 2.5/47.5, and POC-MgO/HA 5/45 (n=8, crosslinked at 3d 80ºC, 3d 120ºC vacuum) were placed in tubes with 10 mL 1X PBS buffer and incubated at 37ºC. At time points of 1d, 3d, 7d, and 14d, the PBS solution was removed and the pH of the solution was tested using a pH meter.

2.12 Swelling Study

The relative swelling of magnesium oxide doped composites was characterized by weighing 7mm diameter, 1mm thick disks of POC/HA, POC-MgO/HA 1/49, POC-MgO/HA 2.5/47.5, and POC-MgO/HA 5/45 (n=8, crosslinked at 3d 80ºC, 3d 120ºC vacuum) and placing them in 10 mL deionized (DI) water at 37ºC. At time points of 1d, 3d, 7d, 14d, and 21d the water was removed and the disks patted dry and weighed. After weighing the disks were placed in 10mL fresh DI water. Swelling was calculated according to Equation 2.

Equation 2:

$$\% \text{ Mass increase} = [(\text{Final Sample weight})/(\text{Initial Sample Weight})] \times 100$$

2.13 Self-setting Characterization of CUPE, BPLP, and POC-click

The self-setting ability of magnesium oxide was explored briefly in other polymers of the citrate-based polymer family including BPLP, CUPE, and POC-click. BPLP and POC-click were synthesized and purified according to our previous work. The setting times of these polymers were characterized as described above (See Setting Time Determination). For CUPE, 50wt% POC 1:1.1 was combined with

hexamethylene diisocyanate (HDI) to form urethane bonds and vortexed for 30 seconds prior to HA and MgO mixing. Compressive cylinder samples were fabricated as above and tested according to ASTM standards (see Mechanical Property Characterization).

2.14 Statistical Methods

All experiments were performed with multiple trials (n=8, indicated in figures) and values were reported as a mean +/- standard deviation (SD). ANOVA was used to determine statistical difference between groups, with significance at $p<0.05$.

Chapter 3

Results

3.1 Setting Time Determination

The setting time of various POC-MgO compositions were determined at a range of temperatures to gain an initial understanding of temperature's effect on the setting times *(Note: System compositions will follow POC[A:B](X)-MgO(Y)HA(Z) convention, where [A:B] is the citric acid:octanediol ratio, X is POC prepolymer solution wt%, Y is MgO wt%, and Z is HA wt%. If [A:B] is not included, citric acid:octandiol is 1:1. Example formulations described in Materials and Methods).* A constant POC solution concentration of 30wt% in ethanol was used for the initial temperature testing, with 10wt% MgO of the final composite. Temperature was found to be a major factor in the setting time of the material. For POC(30)-MgO(10) the average setting time at room temperature (24^{o}C) was found to be 104 minutes. This was significantly higher than the setting time at body temperature (37^{o}C) of 24 minutes. Setting times at 50^{o}C, 75^{o}C, 100^{o}C, 150^{o}C, and 200^{o}C were 16.3 minutes, 4.5 minutes, 3.9 minutes, 2.3 minutes, and 1.9 minutes respectively. Figure 3A shows the temperature dependent setting response for POC(30)-MgO(10). Single factor ANOVA statistical analysis of the temperature dependent effect of setting time returned a p value of 8.61E-32, indicating a clear statistical significance of temperature on setting time.

The concentration of the POC prepolymer solution was found to have a significant effect on the setting time of the material due to changing the amount of solvent (ethanol) in the system (Fig. 3B). POC prepolymer solutions of 40wt% and 50wt% were used in addition to the standard 30wt% solution in the POC(30)-MgO(10) system. For a 40wt% POC solution in the POC(40)-MgO(10) system, setting times at room temperature, body temperature, and 75^{o}C were found to be 46 minutes, 13.4 minutes, and 2.9 minutes respectively. For a 50wt% POC solution in the POC(50)-MgO(10) system, setting times for

26ºC, 37ºC, and 75ºC were 37.8 minutes, 11.6 minutes, and 2.75 minutes. Single factor ANOVA evaluated at all three temperatures showed a statistical significance between the three concentrations of prepolymer. At room temperature ANOVA returned p=7.9E-11, p=1.6E-9 at body temperature, and p=2.93E-7 at 75ºC.

The concentration of MgO in the system was also a significant factor in the setting time of the material (Fig. 3C). For POC(30)-MgO(10) the setting times were 104 minutes, 24 minutes, and 8.9 minutes for room temperature, body temperature, and 75ºC. For POC(30)-MgO(5), at 26C, 37C, and 75C, the setting times were 319 minutes, 88 minutes, and 8.9 minutes for room temperature, body temperature, and 75ºC. For a higher MgO concentration of 15wt%, POC(30)-MgO(15) had setting times of 112 minutes, 40 minutes, and 5 minutes for room temperature, body temperature, and 75ºC. It's worth noting that there is in fact a significant increase in setting time from the POC(30)-MgO(10) system to the POC(30)-MgO(15) system, which was not expected due to the initial observation that a higher concentration of MgO speeds up the setting process. Single factor ANOVA showed statistical significance between the three MgO concentrations at all three temperatures with p=4.44E-12 at room temperature, p=5.72E-13 at body temperature, and p=4.51E-10 at 75ºC.

Different POC prepolymer compositions were used to further test the setting time of POC-MgO composites. As described by our previous work, POC can be synthesized with a variety of monomer ratios; POC, as written, is understood to be a 1:1 ratio of citric acid and 1,8-octanediol monomers, but ratios of 1:1.1, 1:1.3, 1.1:1, and 1.3:1 [citric acid:octanediol] can all also be used (these compositions are written as POC[1:1.1], POC[1:1.3], etc...). With prepolymer solutions held at 30wt% and MgO at 10% total weight (POC(30)-MgO(10)), Figure 3D shows the variation in setting time between these different compositions of POC. POC[1.1:1](30)-MgO(10) showed the highest setting times of all compositions, with a room temperature setting time of 217 minutes. This was significantly higher than all other POC compositions at room temperature (40 minutes, 66 minutes, and 100 minutes for POC[1:1.1](30)-MgO(10), POC[1:1.3](30)-MgO(10), and POC[1.3:1](30)-MgO(10) respectively, single factor ANOVA

p=6.61E-17). The variation in the setting time was most obvious at these lower temperatures, with setting times becoming much closer at the 37ºC and 75ºC test temperatures. At 37ºC, single factor ANOVA again rejected the null hypothesis and indicated statistical significance between groups with p=2.7E-14. At 75C, POC[1:1.1](30)-MgO(10), POC[1:1.3](30)-MgO(10), and POC[1.3:1](30)-MgO(10) were all within 1.5 minutes of each other (2.9 minutes, 4.1 minutes, and 4.4 minutes respectively), but ANOVA again indicated statistical significance with p=1.11E-6. Again, POC[1.1:1](30)-MgO(10) showed the highest setting time of 7.4 minutes at 75ºC.

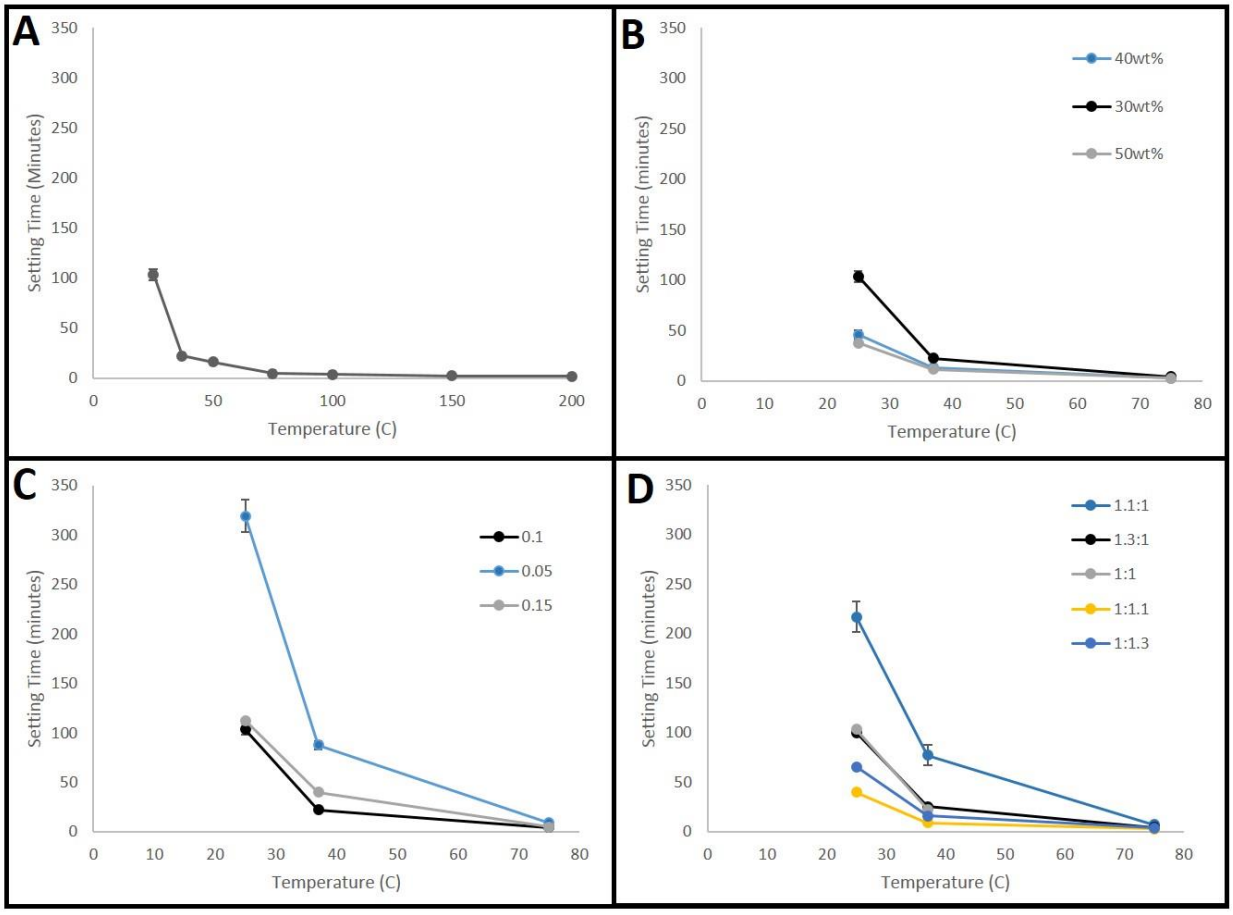

Figure 3: Setting times for POC-MgO systems. POC(30)-MgO(10) in Fig.3A., POC(X)-MgO(10) in Fig.3B, POC(30)-MgO(X) in Fig.3C, and POC[A:B](30)-MgO(10) in Fig.3D. All four of these factors were shown to have a significant effect on the setting time of the material. Changing the composition of the material allows for modulation of the setting time from over 100 minutes to less than 2 minutes. This variation allows for optimization of setting time depending on the application.

In addition to prepolymer solution concentrations, MgO concentration, and POC monomer ratio, the addition of ceramic to the material was also shown to have a significant effect on the setting time of the material. Hydroxyapatite was added at fractions of the total material weight ranging from 15wt% to 55wt%. Figure 4 shows the temperature dependent setting times of HA containing composites, with a constant 50wt% POC[1:1] prepolymer solution and MgO(5). At room temperature there was no statistically significant difference between the six compositions, with setting times all within the 10.2-10.5-minute range (single factor ANOVA with p=0.94). At body temperature, setting times dropped to the 3.7-5.1-minute range, with statistical significance between groups (p=1.81E-7). Setting at 75°C showed a range of 1.5-2.8 minutes, again with statistical significance between groups via single factor ANOVA (p=5.25E-10). Generally, setting times were slightly decreased in higher percentage HA containing composites, although only by a maximum of 1.4 minutes between POC(50)-MgO(5)-HA(15) and POC(50)-MgO(5)-HA(55) at 37°C.

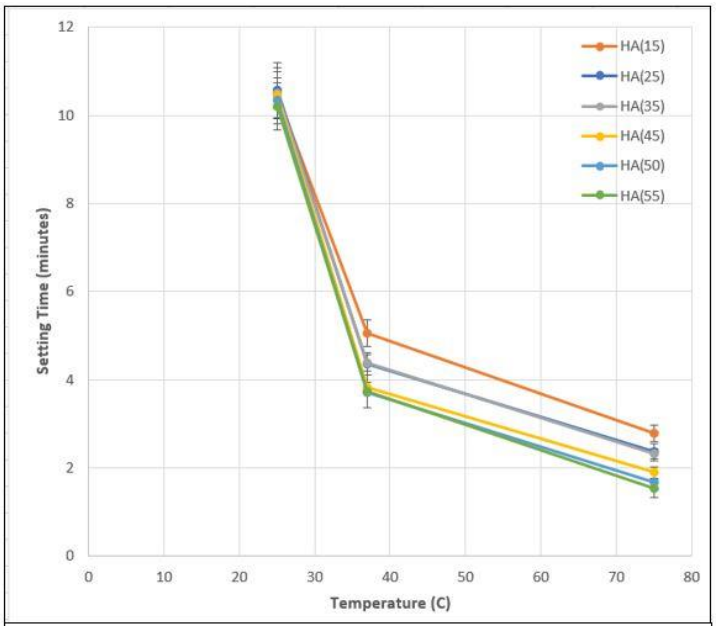

Figure 4: Setting times for POC-MgO-HA systems. POC(50)-MgO(5)HA(X) systems showed little variation between HA amounts, but a much lower overall setting time than non HA systems. Variation of HA content of material allows for the optimization of setting time for bone specific MgO doped POC/HA composites.

3.2 Factor Analysis Setting Time Model

The program Design-Ease (Stat-Ease Inc., Minneapolis) was used to develop a multi-factor setting time model from the collected setting time data. All setting time data is reported in Table 3. The Appendix shows the model predicted setting time values for a full experimentally measured set of data (Fig. 22) and for a set with only experimentally measured data for the 10wt% MgO composition. Bar height indicates the predicted setting time and red dots indicate the experimentally determined setting times. The full model predictive equation and factor analysis ANOVA are listed in the Appendix, along with a verification of the setting time model with one unused formulation (POC-MgO 1.3:1 50wt% POC, 5wt% MgO, Fig. 23). At low temperature the model was statistically inaccurate, however at 37^{o}C and 75^{o}C the model was accurate to the experimentally tested setting time.

These setting time results indicate the ability of MgO to modulate the setting time from in excess of hours to under 2 minutes depending on the formulation of the material and the setting temperature. This raw data was used to create a factor analysis predictive model for the setting time. The ability to quantitatively predict the setting time for any formulation of the above factors gives a valuable tool for scaling the manufacture of these materials through either injection molding, or in the future 3D printing.

Table 3: Full setting time data. Reported value is average of 5 trials.

	Average Setting Time (minutes) at:		
Material Composition	**26C**	**37C**	**75C**
POC(30)-MgO(5)	319	87.8	8.9
POC(40)-MgO(5)	113	28	4.4
POC(50)-MgO(5)	105	20.2	3.8
POC(30)-MgO(10)	104	22.4	4.5
POC(40)-MgO(10)	46	13.4	2.9
POC(50)-MgO(10)	38	11.6	2.8
POC(30)-MgO(15)	112	40.1	5.1
POC(40)-MgO(15)	93.6	24	3.2
POC(50)-MgO(15)	57	15.4	2.4
POC[1:1.1](30)-MgO(10)	40	9.3	2.9
POC[1:1.3](30)-MgO(10)	66	16.1	4.1
POC[1:1.3](40)-MgO(10)	43.8	13.3	2.9
POC[1:1.3](50)-MgO(10)	30.3	11.2	2.4
POC[1.1:1](30)-MgO(10)	217	77.4	7.4
POC[1.1:1](40)-MgO(10)	149	33	5.2
POC[1.1:1](50)-MgO(10)	115	24.8	4.2
POC[1.3:1](30)-MgO(10)	100	25.4	4.4
POC[1.3:1](40)-MgO(10)	49	10.7	3.02
POC[1.3:1](50)-MgO(10)	37.3	7.3	1.99
POC(50)-MgO(5)-HA(15)	10.5	5.1	2.8
POC(50)-MgO(5)-HA(25)	10.5	4.4	2.4
POC(50)-MgO(5)-HA(35)	10.5	4.4	2.3
POC(50)-MgO(5)-HA(45)	10.4	3.8	1.9
POC(50)-MgO(5)-HA(50)	10.3	3.7	1.7
POC(50)-MgO(5)-HA(55)	10.2	3.7	1.5

3.3 Mechanical Characterization

The compressive peak stress, compressive (Young's) modulus, and strain at fracture were characterized by standard ASTM compressive testing procedures and POC/HA groups with low levels of MgO were shown to have almost double the peak stress of POC/HA controls as well as a Young's modulus closer to that of natural bone. Six groups of POC(50)-MgO(5)-HA(55) were tested: 1 hour mold

with no thermal crosslinking, 1 hour mold time with 3 days 80C crosslinking, 1 day mold time with no thermal crosslinking, 1 day mold time with 3 days 80°C crosslinking, 3 days mold time, and 3 days mold time with 3 days 80°C crosslinking. Figure 5A shows the peak compressive stress in these samples with standard deviation. A t-test showed a statistically significance difference between the peak stress of samples crosslinked at 80°C and no thermal crosslinking ($p<0.05$). Of the six groups, a 3 day mold time without thermal crosslinking showed the highest average peak compressive stress at 32.2 MPa. The lowest compressive peak stress was seen in the 1-hour mold, with 3 days 80°C thermal crosslinking at 16.7 MPa. POC-HA 60wt% control samples were also tested; one group was thermally crosslinked at 80C for three days and one was not thermally crosslinked. Young's Modulus was significantly higher in all three molding time POC-MgO/HA 5-55 composites than the POC/HA control (Fig. 5B, $p<0.05$). There was no significant difference in Young's Modulus between the different mold times. POC/HA controls had a modulus of 0.2 GPa, while 5wt% MgO containing composites saw an increase to ~1 GPa. Peak strain was significantly lower than the POC/HA control for 1 hour and 1 day mold times for the POC-MgO/HA 5/55 composites ($p<0.05$), with these composites only reaching a strain of 2-6% before failure (Fig. 5C). There was no significant difference between the molding times in peak strain at failure. Although the Young's modulus was improved in the MgO doped group, the overall mechanical properties were still lacking, prompting the characterization of several other formulations.

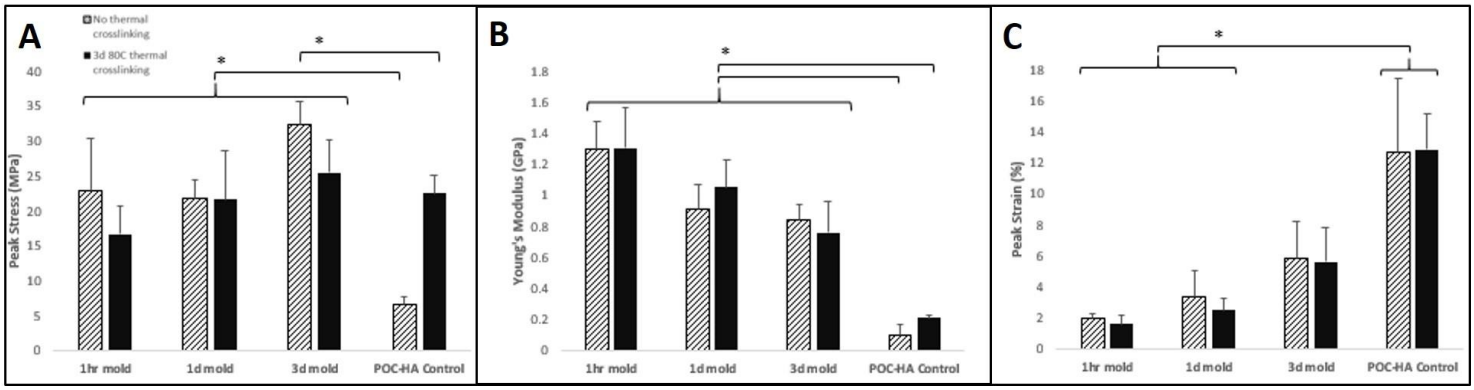

Figure 5: POC-MgO/HA 5/55 Mechanical Data. Subfigure A shows peak stress, Subfigure B shows Young's Modulus, Subfigure C shows peak strain. Solid bars indicate 3d 80°C thermal crosslinking while striped bars are tested without thermal crosslinking. At this material formulation the peak stress was not significantly higher than the crosslinked POC/HA control, indicating the need for a different formulation of the material. * indicates $p<0.01$

The peak compressive stress and compressive modulus of 2.5wt% MgO composites was also determined, and in this case shown to have improved properties from the 5wt% MgO composites. POC(50)-MgO(2.5)HA(57.5) cylinders were fabricated and tested with the same parameters as POC(50)-MgO(5)HA(55) cylinders (Fig. 6). Compressive strength was significantly higher in the POC(50)-MgO(2.5)HA(57.5) composites, with 1d mold no thermal crosslinking at 54.2 MPa, 1dm 3d 80ºC at 57.2 MPa, 3d mold no thermal crosslinking at 53.9 MPa, and 3dm 3d 80ºC at 63.2 MPa. Compared to the POC-HA controls again, these values were significantly higher, with $p<0.02$. The compressive moduli of the POC(50)-MgO(2.5)HA(57.5) composites were not significantly different than the POC(5)-MgO(5)HA(55) composites. With no thermal crosslinking, 1-day mold composites had a modulus of 0.93 GPa and 3 day mold composites had a modulus of 0.89 GPa. With thermal crosslinking 1 day mold composites had a modulus of 1.01 GPa, and 3 day mold composites had a modulus of 0.87 GPa. The compressive moduli of all POC(50)-MgO(2.5)HA(57.5) composites were significantly higher than POC/HA controls ($p<0.02$). The peak strain of POC(50)-MgO(2.5)HA(57.5) composites were slightly higher than POC(50)-MgO(5)HA(55) composites, ranging from 7% to 11% at break, and not significantly different than POC/HA controls. From these results, the mold time was chosen to remain at 1 day in future groups and the 1 hour and 3 day mold times were excluded.

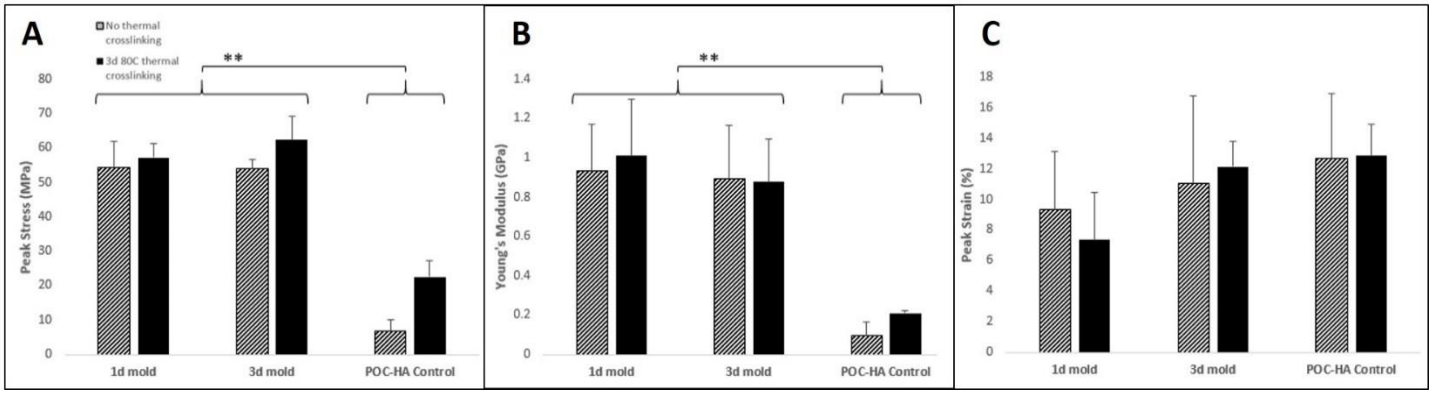

Figure 6: POC-MgO/HA 2.5/57.5 Mechanical Data. Subfigure A shows peak stress, subfigure B shows Young's Modulus, subfigure C shows peak strain. Dark bar indicates 3d 80ºC thermal crosslinking while striped bar indicates no thermal crosslinking before testing. By decreasing the amount of MgO to 2.5wt%, the peak stress was significantly improved to more than double that of the control. The Young's modulus was also maintained at a higher level than the control. ** indicates $p<0.02$.

As the previous data suggested, the 1 hour and 3-day mold times were unneeded, thus for the 1wt% MgO group only the 1 day mold time was tested, Additionally, to match the mechanical properties of the MgO doped groups to the best configuration of the control group (POC/HA), an additional crosslinking condition of 1dm, 3d 80ºC, 3d 120ºC vacuum was tested for all 60wt% ceramic composites. The POC(50)-MgO(1)HA(59) group showed similar peak stress and Young's modulus to POC(50)-MgO(2.5)HA(57.5) at the 1dm and 1dm 3d 80C crosslinking conditions. As expected, the decreased MgO concentration in the POC(50)-MgO(1)HA(59) composites slightly increased the peak strain, but also lowered the Young's modulus from the POC(50)-MgO(5)HA(55) formulation. The additional crosslinking condition of 1dm, 3d 80ºC, 3d 120ºC vacuum did little to change the material properties of the MgO containing composites, only slightly increasing the peak stress. The additional crosslinking at 120ºC had strongest effect on the POC/HA controls, which indicates why that crosslinking condition was initially tested. Overall, the full set of data at 60wt% ceramic indicates that the best crosslinking condition for these materials is the 1dm, 3d 80ºC, 3d 120ºC vacuum, however the mechanical properties were still thought to be improvable, prompting another set of testing with a lower ceramic amount.

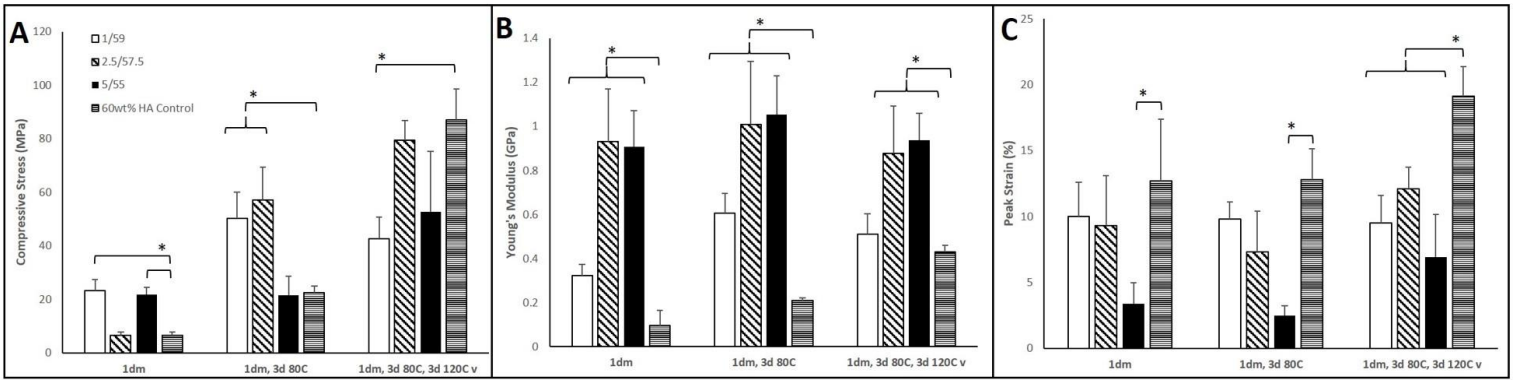

Figure 7: Full 60wt% ceramic composite mechanical data. Subfigure A shows peak stress, subfigure B shows Young's Modulus, subfigure C shows peak strain. Mold time was kept constant at 1 day, and the highest peak stress were seen in all composites at the 1dm, 3d 80ºC, 3d 120ºC vacuum crosslinking condition. Although Young's modulus was still improved from the POC/HA control, peak stress was not significantly improved, prompting the need for a different formulation of the MgO doped POC/HA material. (* indicates $p<0.05$).

To better balance the added brittleness of the MgO, the total amount of ceramic in the composite was reduced to 50wt% and the mechanical properties were re-characterized, showing an again improved peak stress and the "ideal" formulation of the material. Fig. 8 shows the full set of peak stress, young's modulus, and peak strain for all tested composites at the 1dm, 3d 80ºC, 3d 120ºC vacuum crosslinking condition. This data set shows the clear improvement of mechanical properties when the total ceramic amount is reduced from 60wt% to 50wt%. For 1/49 and 2.5/47.5 MgO containing groups, the peak stress exceeded 200 MPa with Young's moduli still around 1 GPa. Additionally, the peak strain of the 1/49 group matches that of the POC/HA control, further indicating the ability to maintain and improve the mechanical properties of the material.

The mechanical characterization of MgO doped materials ranging from 1wt% to 5wt% at a total ceramic amount of 50wt% and 60wt% indicates that a lower amount of MgO, and a ceramic amount of 50wt% provides the best peak stress and Young's modulus. 1wt% and 2.5wt% doped MgO POC/HA composites exhibited peak stress above 200 MPa and moduli of 1GPa, both significant improvements on POC/HA controls and within the range of cortical bone. These formulations were considered the best of all tested groups and indicates a possibility for use of these composites in load-bearing applications.

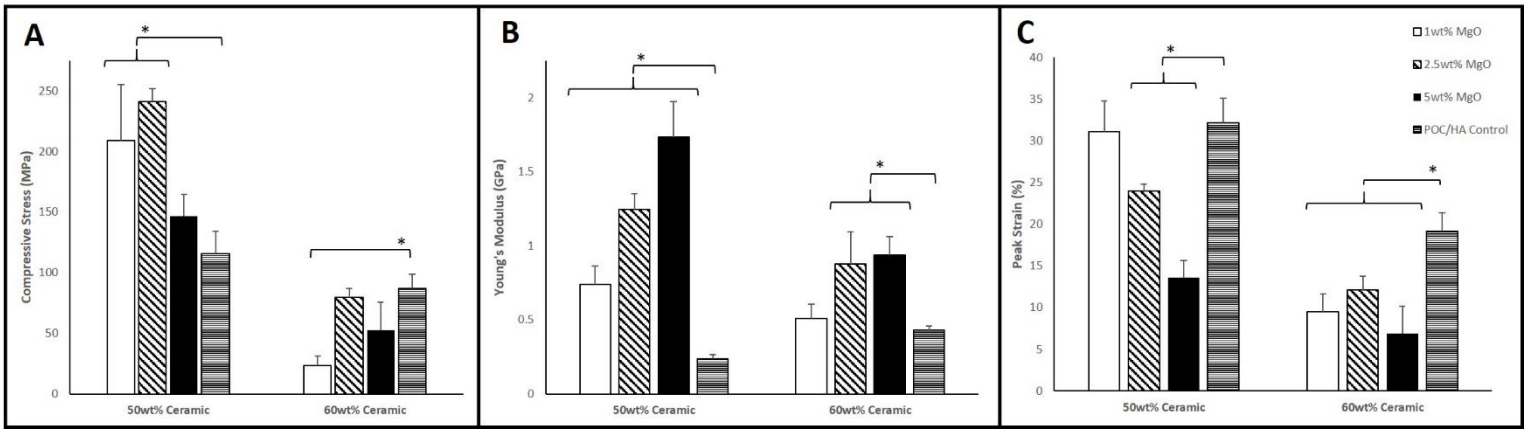

Figure 8: Full Mechanics at 1dm, 3d 80C, 3d 120C vacuum. Subfigure A shows peak stress, subfigure B shows Young's Modulus, subfigure C shows peak strain. 1wt% and 2.5wt% MgO composites at 50wt% ceramic showed the best peak stress and maintained a modulus of about 1GPa. These results indicate a step towards the natural mechanical properties of bone and the potential for these materials to be used in load bearing orthopedic applications. (* indicates $p<0.05$).

3.4 Density and Size Verification

The density of the various compositions of POC-MgO were compared to prove the ability to fabricate the material at a consistent crosslinking density through the injection molding process. Table 4 shows the density of several of these groups. Notably, the average density of the materials all are within the 1.26 to 1.33 mg/mm^3 range, indicating a replicable density from the injection molding of the cylinders. Single factor ANOVA on the density data showed a p value of 0.42, indicating an acceptance of the null hypothesis (i.e. there is no statistically significant difference between groups). This analysis shows the consistent fabrication of cylinders despite different compositions.

Table 4: Density Verification of POC-MgO/HA composites. Single factor ANOVA showed no significant difference between the groups.

	Density (mg/mm^3)
POC(30)-MgO(5)	1.33 +/- 0.06
POC(30)-MgO(10)	1.26 +/- 0.05
POC(30)-MgO(15)	1.28 +/- 0.03
POC(40)-MgO(10)	1.29 +/- 0.04
POC(50)-MgO(10)	1.28 +/- 0.05

In addition to confirming the density of MgO doped composites, the size of the composites before and after crosslinking was determined to confirm that any shrinkage of the material was isotropic. As shown by Fig. 9, all three MgO doped POC/HA composites showed shrinkage after crosslinking by about 4-5%. This amount of shrinkage was not seen in the POC/HA composite. Although shrinkage in general is unwanted, in this case the percent change seems to be isotropic (no statistical difference between diameter and length change, $p>0.05$), indicating that this could be controlled for in the fabrication process. In general, the fabrication limitations of MgO doped POC/HA due to shrinkage are controllable, and even in rudimentary manual injection molding the density of the material is maintained. Both of these potential setbacks are highly controllable.

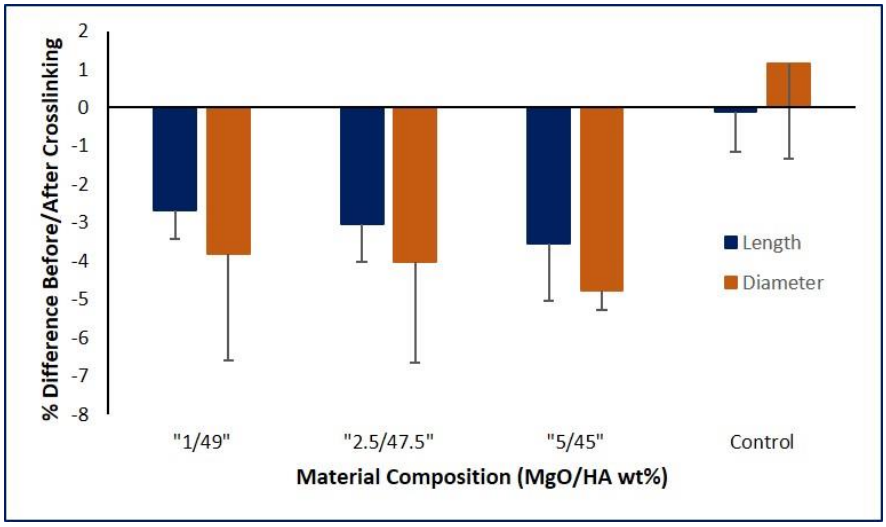

Figure 9: Sample Size change before/after crosslinking. Control is 50wt% POC/HA, experimental groups are POC-MgO(1)HA(49), POC-MgO(2.5)HA(47.5), and POC-MgO(5)HA(45). There is no significant difference between length and diameter % difference for any MgO containing groups, indicating controllable isotropic shrinkage of the material ($p>0.05$).

3.5 Injection Molding

Initial injection molding of POC-MgO/HA composites resulted in both solid geometries and porous scaffold geometries which were previously unattainable with standard POC/HA composites. Mold geometry of the temporomandibular joint was extracted from an X-ray scan of the skull using MIMICs and processed with Solidworks. Fig. 10 shows the scan, CAD design of the mold, and 3D printed mold. 2.5wt% MgO doped POC/HA was injected into the mold and allowed to set for 1 day. Once removed from the mold, the composite material was shown to have retained with high accuracy the smaller feature geometries of the mold, including the 200um filament layers from the 3D printer. A second 3D printed mold with higher resolution was created and a more detailed injection molded composite created (Fig. 10G). The ease of fabrication of the MgO doped POC/HA material is clear compared to POC/HA without MgO; Fig. 11 shows the result of injection molding POC/HA (Fig. 11B) compared to injection molded POC-MgO/HA (Fig. 11A). The POC/HA material remains a semi-liquid even after one day in the mold, preventing its use as an injection molding material.

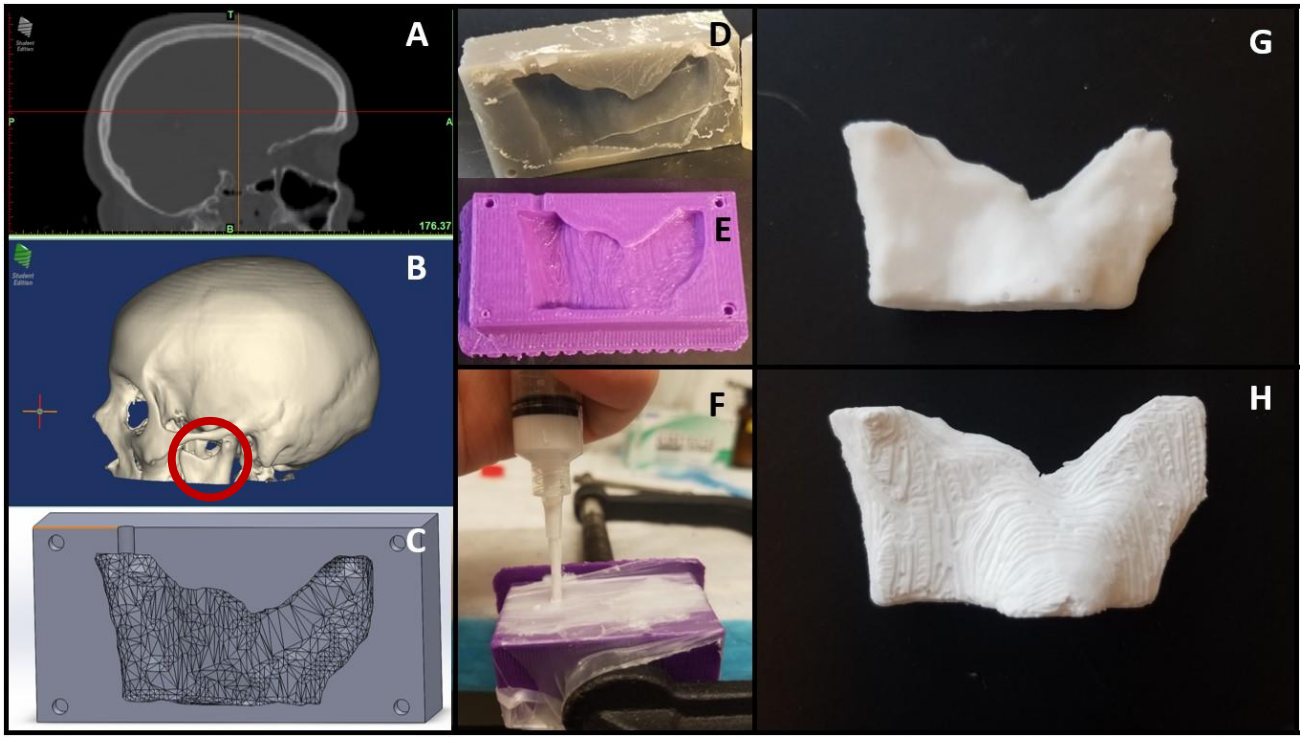

Figure 10: Injection Molding Workflow. Coronoid process and temporomandibular joint was extracted from scan of skull and converted into 3D printable mold. POC-MgO/HA 2.5/47.5 was molded in both 3D printed molds and retained high accuracy of the mold shape (D,E).

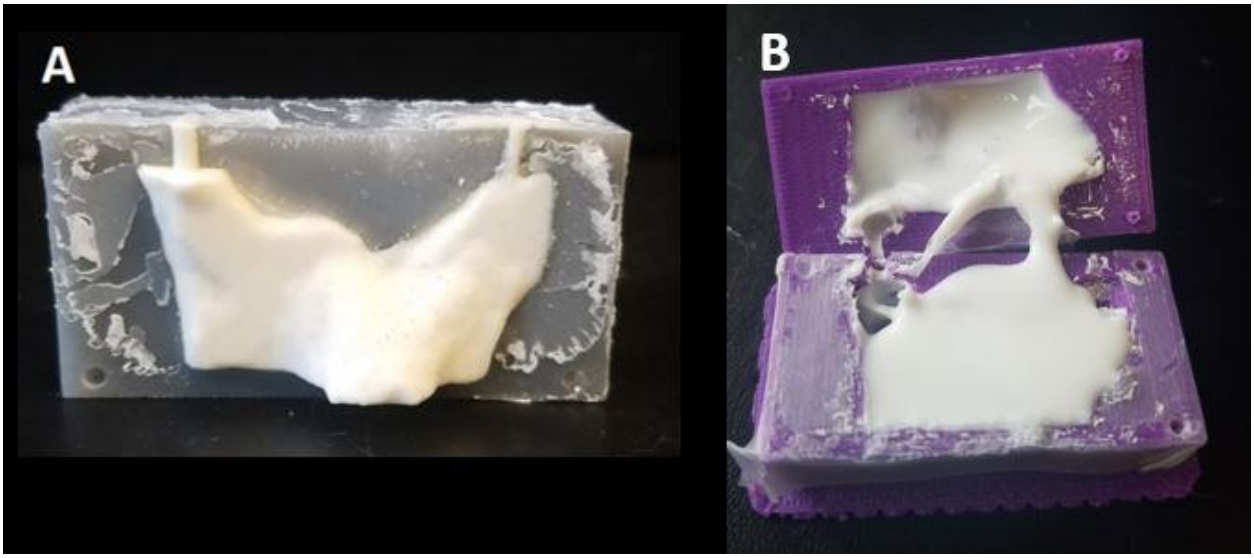

Figure 11: Injection molding comparison of MgO doped and MgO free POC/HA materials. Subfigure A shows the retention of mold shape in the MgO doped POC/HA material while subfigure B shows the inability of POC/HA to maintain mold shape due to the lack of self-setting ability.

In addition to complex mold geometries extracted from physiological scans, other simpler geometries were created, largely made possible by the ability of MgO doped POC/HA to retain extremely fine micro-level detail from the mold. Fig. 12 shows fabricated screws, porous scaffolds, and ridged plates also created via injection molding of POC-MgO/HA formulations. Fig. 12A shows a screw with high tolerances which was easily fabricated by molding the material into a preexisting screw mold (d=5mm). Fig. 12B shows a porous scaffold of POC-MgO(2.5)HA(57.5) fabricated by injection molding the material with 40wt% salt and leaching the salt after the material had set in mold for 1 day. The salt was able to be leached without thermally crosslinking the material first. Fig. 12C-E shows a ridge structure on a plate which was made from molding the material into a ridged 3D printed mold. The ridge structure was maintained after crosslinking with high accuracy to the initial 3D printed mold. The ridge depth was 100 um, and the width of each ridge was less than 75 um (scale bar 100 um). The unique ability of MgO doped POC/HA to pick up these fine details indicates the possibility of transferring microarchitecture to the surface of these materials, a characteristic previously impossible with POC/HA.

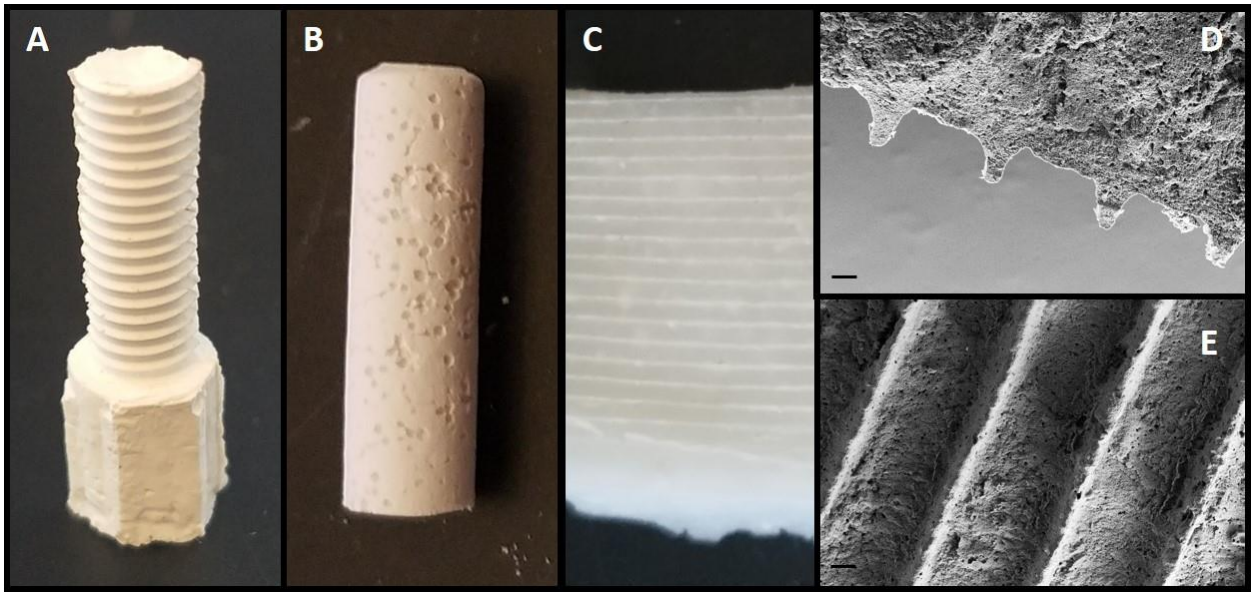

Figure 12: Injection Molding Capabilities. Screws, porous scaffolds, and micro ridged plates were all fabricated with injection molding of MgO doped POC/HA composites. Fine ridge architecture on the microscale provides a unique way to design the surface of the material for specific applications, especially with respect to improving cell attachment and growth. (Scale bar in D,E is 100um).

3.6 Accelerated Degradation

An accelerated degradation test of MgO doped POC/HA composites characterized the relative degradation curve of these materials, showing a slightly increased degradation rate in the MgO doped materials. Figure 13 shows the degradation curve of POC-MgO(1)HA(49), POC-MgO(2.5)HA(47.5), and POC-MgO(5)HA(45) composites compared to a control composite of POC-HA(50wt%). All composites showed a standard curve, with the higher MgO containing composites showing a slightly faster degradation rate. There was no significant difference in the mass loss until day 10, with all MgO containing composites degrading to 20% of their initial mass by this time point. By day 14, all MgO containing composites had degraded to less than 15% of their initial weight, while the control composite was still above 25% of its initial weight. These results indicate little difference between the POC/HA and MgO doped POC/HA, except for a slightly faster degradation at days 10-14.

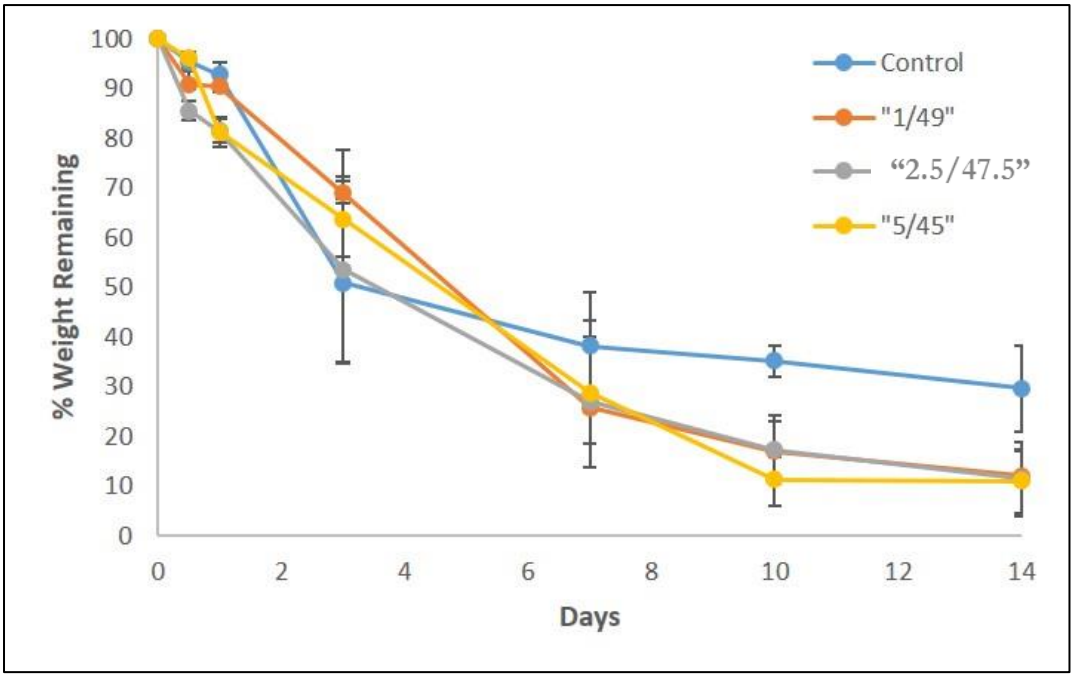

Figure 13: Accelerated Degradation of MgO containing composites (wt% MgO /wt% HA). Degradation was similar for all groups until day 10 and 14, at which MgO doped POC/HA had slightly faster degradation rate. Overall the degradation data suggests suitability in the body. Control composite is 50wt% POC/HA.

3.7 pH Response

The pH response of MgO doped POC/HA composites was tested over a two-week period (Fig. 14) and indicated the improved ability of MgO doped POC/HA to buffer the slightly acidic nature of the citric acid polymer. Initial pH of the test medium was 7.4 (1X PBS). The control POC/HA 50wt% composite showed the most acidic response of the composites, dropping below 7.3 in 1 day. POC-MgO(1)HA(49) and POC-MgO(2.5)HA(47.5) also showed a slight decrease in pH, although only to 7.35 in the first day, demonstrating the buffering ability of the basic MgO. POC-MgO(5)HA(45) never showed a drop in pH, increasing in the first day to 7.55 and maintaining this pH throughout the test. The other MgO containing composites showed an increase to 7.5, along with the control composite by day 10. The buffering ability of the 1wt% and 2.5wt% MgO doped groups is beneficial to the material as it prevents the acidic response seen in the control. However, the 5wt% MgO group overpowers the acidic nature of the polymer and shows a basic response, indicating a poor fit for this group in a physiological application.

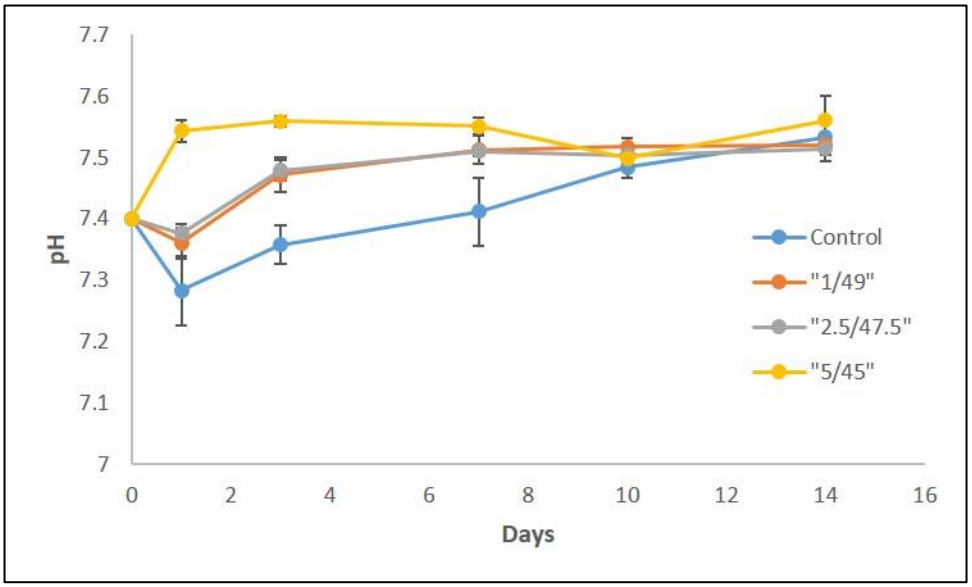

Figure 14: pH response of MgO containing composites. 1wt% and 2.5wt% MgO groups showed an improved ability to buffer the pH closer to 7.4 than both the control (slightly acidic) and the 5wt% MgO group (basic). The 1wt% and 2.5wt% MgO groups illustrate the best response and further support them as the best formulations of the material. Control is POC/HA 50wt%.

3.8 Swelling Testing

The swelling of MgO doped POC/HA composite disks was tested over a two-week period and again indicated that the 1wt% and 2.5wt% MgO groups would be suitable for implantation while the 5wt% MgO group is too much MgO for the system. Fig. 15 shows the swelling response of these composites with a POC/HA 50wt% control. POC-MgO(1)HA(49) and POC-MgO(2.5)HA(47.5) composites showed a statistically similar response to the control, with a slight increase in mass to a steady value of about 15% mass increase. POC-MgO(5)HA(45) showed a larger increase in mass with a 37% mass increase in the first day. A drop in the mass increase in the 5wt% MgO composite is most likely due to its faster degradation compared to the other composites. Again, this response is not ideal and indicates the 5wt% MgO composite is less suitable.

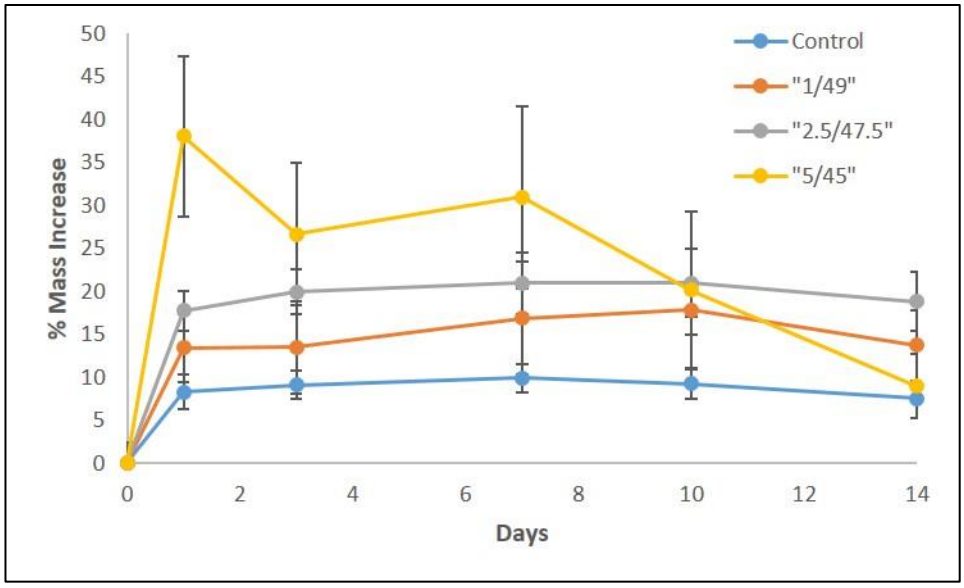

Figure 15: Swelling response of MgO containing composites in distilled water. 1wt% and 2.5wt% MgO groups have similar response to the POC.HA control, while 5wt% MgO shows high swelling and then fast degradation. This indicates that 5wt% MgO is a good upper limit for MgO amount. Control is a POC/HA 50wt% composite.

3.9 Physical Characterization

The physical composition of POC-MgO and POC-MgO/HA composites was determined using FTIR spectroscopy and indicated the chemical binding of magnesium ions to the carboxylic acid groups of citrate in the polymer. Fig. 16 shows the spectra for POC, POC-MgO(15), magnesium citrate tribasic, and magnesium oxide. The most notable changes in the spectra from the POC to POC-MgO are the rounded peaks at 1600 cm^{-1} and 1400 cm^{-1}, and the large spread peak at the low end of the spectrum. The two peaks in the 1600-1400 cm^{-1} range correspond to deprotonated –COOH groups, indicating the binding of magnesium ions to the free citrate carboxylic acid groups in the polymer. This is confirmed by comparing to the magnesium citrate tribasic spectrum which also has these characteristic peaks. The large peak in the 400 cm^{-1} range is due to magnesium oxide; although magnesium citrate tribasic has some artifacts in that region, the large sloping peak is clearly that of MgO. This indicates the presence of both magnesium ions and magnesium oxide in the POC-MgO material, lending some information as to the binding mechanism of the particles in the polymer. We propose that MgO reacts with the pendant geometry of the citrate –COOH groups in the form of magnesium ions, and once those groups have been saturated the remaining magnesium exists as the magnesium oxide species. This explains the self-setting ability of MgO in POC and indicates that this same mechanism would allow for the setting of all other citrate-based polymers, suggesting a much broader impact of this research than just doping POC/HA composites.

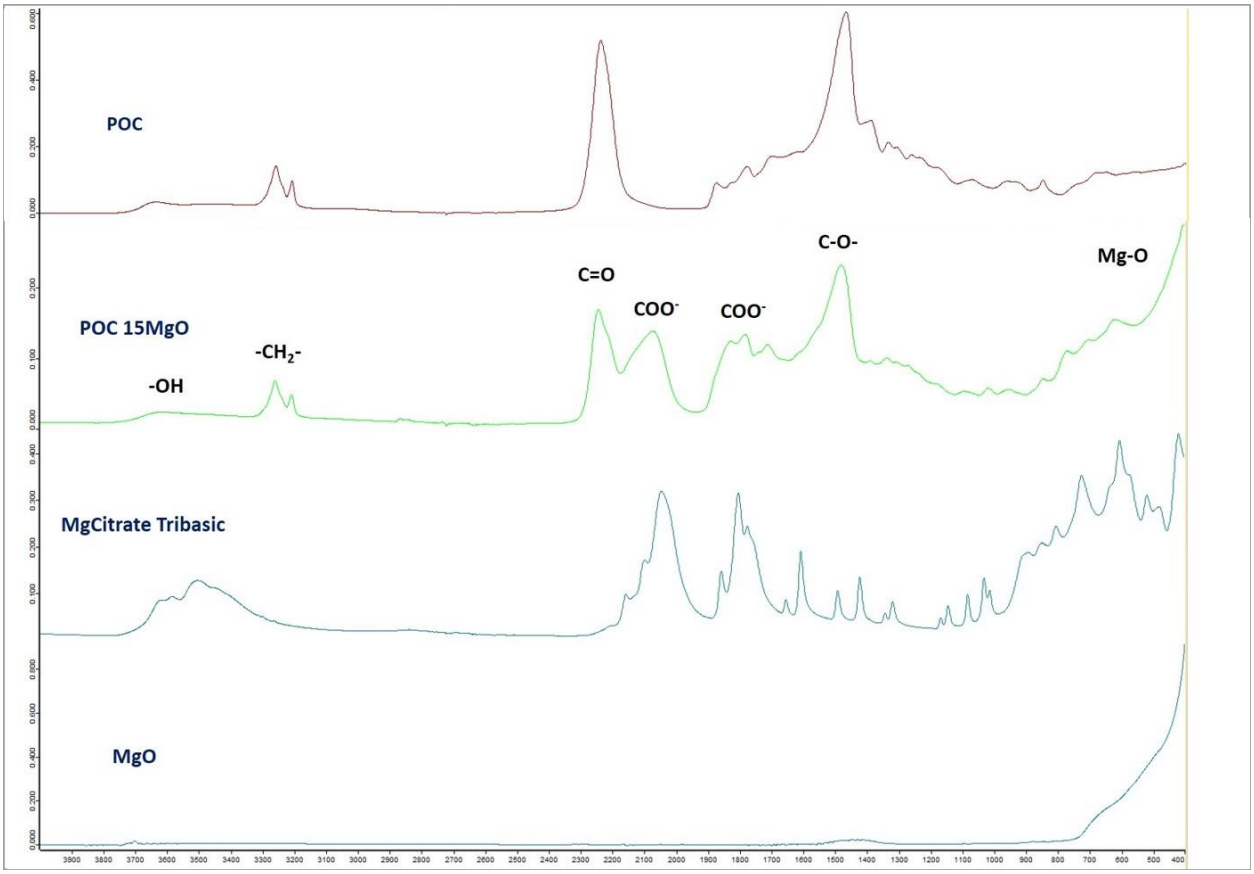

Figure 16: FTIR spectrum of POC, POC-MgO(15), magnesium citrate tribasic, and magnesium oxide. Characteristic peaks in the 1400-1600 cm^{-1} range indicates magnesium ion binding to citrate, while a large peak in the 400 cm^{-1} range indicates the presence of MgO in the system. This suggests a saturation of the citrate with magnesium, explaining the diminishing returns of decrease in setting time with increased MgO amount.

3.10 Mineralization

Mineralization results show unique mineral growth morphology on MgO containing composites when compared to POC/HA controls. POC/HA control disks showed characteristic rounded mineral growth continuing from day 1 to day 7 (Fig. 17). In all three groups containing MgO (1/49, 2.5/47.5, and 5/45), day 1 results show cube-like mineral growth in addition to the rounded growth seen on the control (Fig. 18A). Additionally, by day 7, MgO doped disks show long, thread-like mineral deposition on top of the layered rounded and cube growth (Fig. 18C,D). This type of mineralization was not seen on the

POC/HA control plates. A higher magnification of the mineral growth also shows a honeycomb-like pattern surrounding the cube minerals at day 1, and this same porous growth layered with strand growth at day 7. (Fig. 18B,D). This unique mineral morphology could prove to be excellent for cell growth and attachment, as the porous nature of the mineral growth could encourage cell infiltration, and micro threads are often used in biomaterials to improve cell attachment. The difference in morphology could be due to release of MgO from the material which then redeposits as MgO crystals (cubic), and threads or porous platelets (Ca/Mg-phosphate).

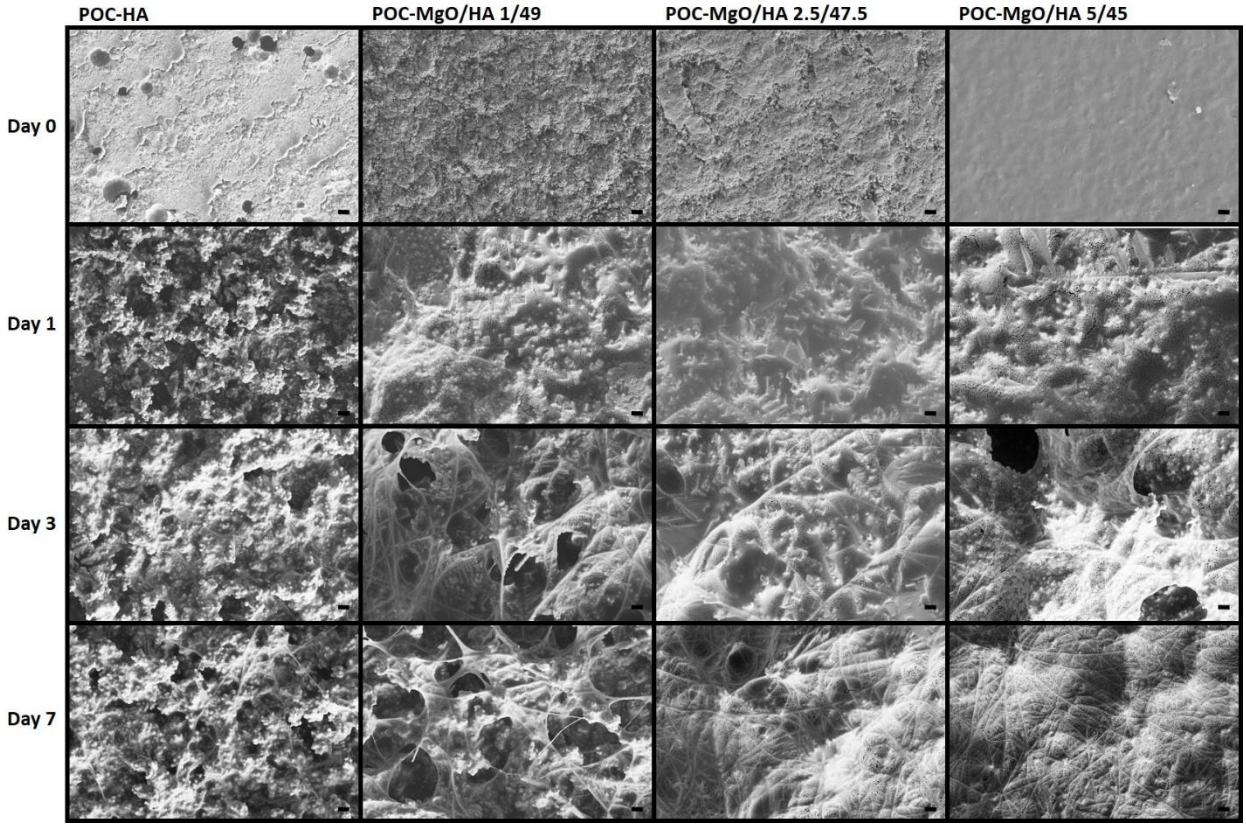

Figure 17: Mineralization of MgO doped POC/HA composites. Control (POC/HA 50wt%) shows rounded amorphous mineral growth while MgO doped composites show thread-like, cube-like porous growth. Porous and thread-like growth on MgO doped POC/HA could encourage cell attachment and growth, indicating a potential imrpvoement on the control POC/HA material. Scale bar 20um.

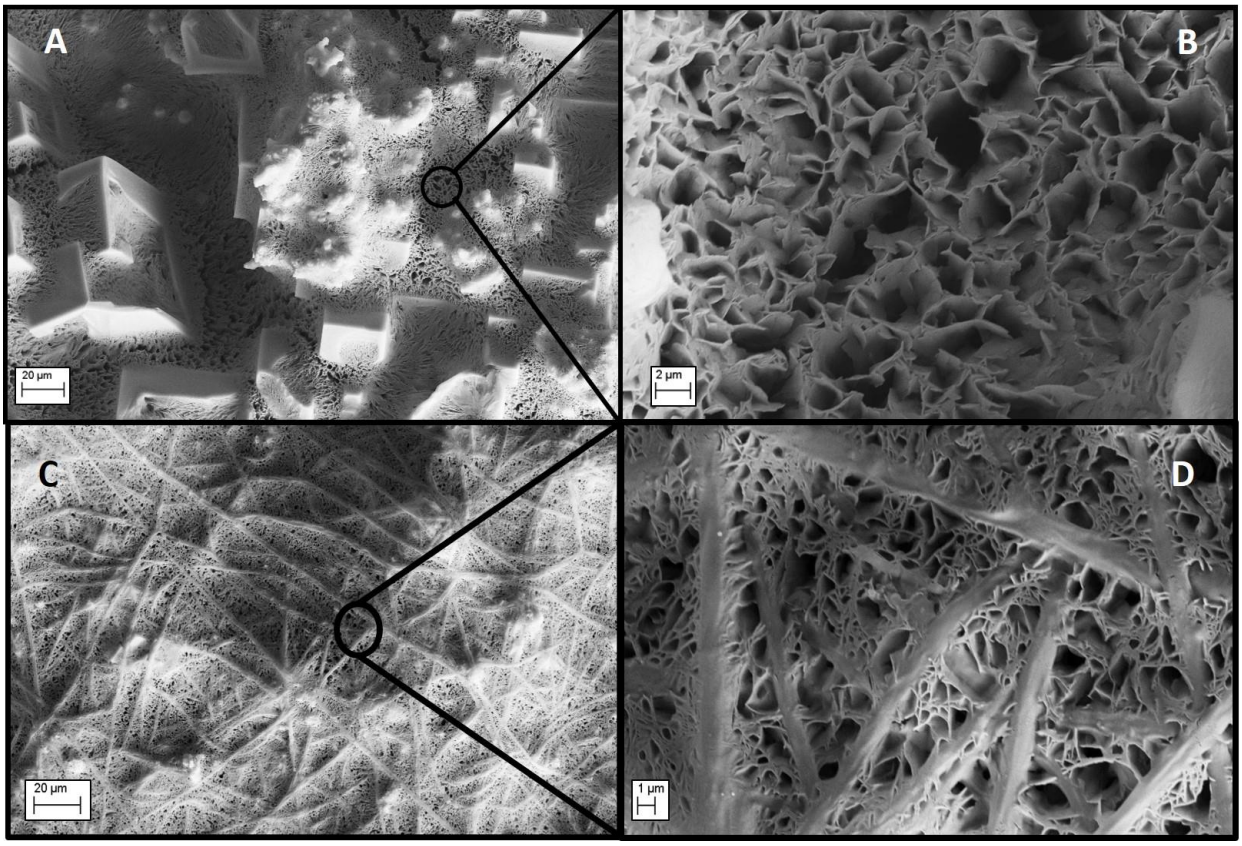

Figure 18: Cubic, thread-like, and porous mineral growth on 5wt% MgO doped POC/HA. Subfigures A, B taken after 1 day of mineral growth and clearly illustrate the cubic growth of magnesium oxide and deep pores. Subfigures C, D taken at day 7 show the layering of threads over the porous minerals.

3.11 Cytotoxicity

The cytotoxicity of MgO doped films was determined via a 24hr CCK-8 cytotoxicity assay and was shown to be comparable to both POC/HA control films and PLGA 75:25 control films. Fig. 19 shows the normalized cell viability on POC-MgO(1)HA(49), POC-MgO(2.5)HA(47.5), and POC-MgO(5)HA(45) vs controls of POC/HA 50wt% and PLGA films. In all groups the cell viability did not drop below 75%, with the PLGA control displaying the highest viability along with POC-MgO(1)HA(49). POC-MgO(5)HA(45) showed the lowest cell viability of the experimental groups,

indicating that increasing MgO may increase cytotoxicity. However, at the levels used in these experimental composites, the overall viability was high enough in all cases to suggest that MgO in lower concentrations does not limit cell viability.

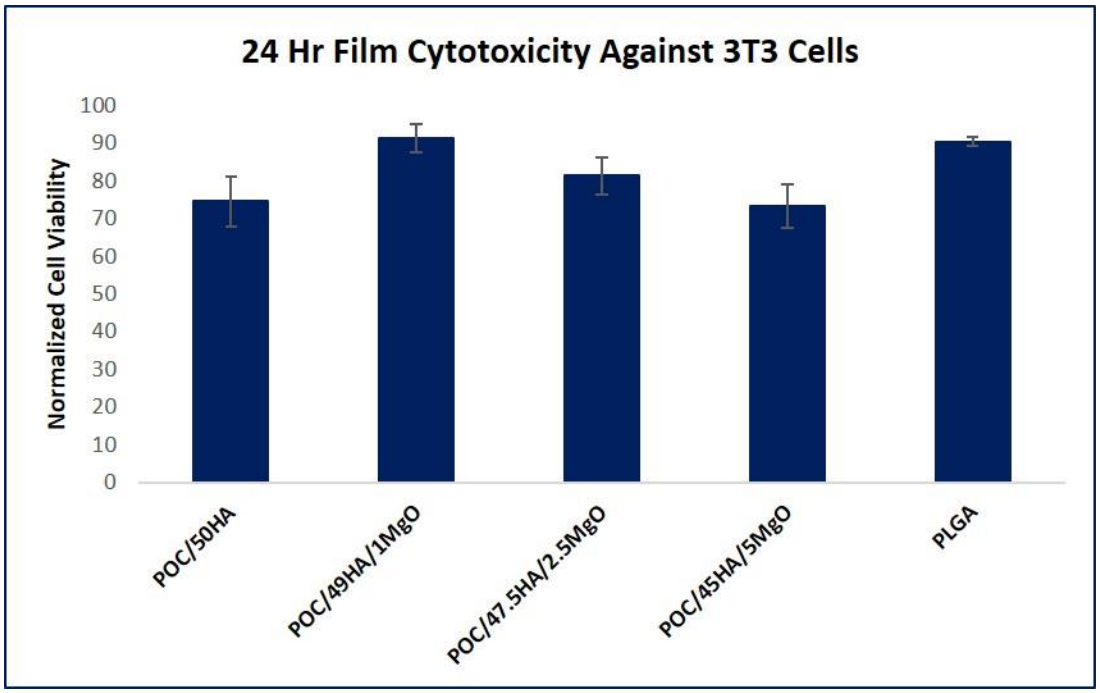

Figure 19: 24-hour film cytotoxicity against 3T3 cells. Normalized cell viability is shown for all groups including PLGA and POC-HA 50wt% controls, with MgO doped POC/HA composites showing comparable cell viability to both controls. A slight decrease in viability was seen at the 5wt% MgO composite, indicating that there is an upper limit for MgO in these materials with respect to cell viability.

3.12 Translation to Other Citrate-Based Polymers

In addition to exploring the applicability of MgO to POC/HA bone composites, the ability of MgO to self-set other polymers in the citrate family was briefly examined to determine other potential applications for MgO use. Fig. 20 shows the setting times for POC-click 0.03-Al, POC-click 0.03-N_3, POC-click 0.03 2:1 Al:N_3, BPLP-ser 0.02, and BPLP-cys 0.02 all with 5wt% MgO and at 75°C. Additionally, POC-click 0.03 2:1 Al:N_3, BPLP-ser 0.02, and BPLP-cys 0.02 with 5wt% MgO and 45wt% HA were also tested. These setting times are all reported in Fig. 20. The ability of MgO to set these other

polymers in a similar amount of time to POC indicates a similar, if not identical mechanism of setting. MgO was also doped into CUPE/HA composites and the mechanical properties of the CUPE-MgO/HA material were shown to be similar to POC-MgO/HA composites (Appendix B, Fig. 24). The wide-ranging applications of these other polymers, including imaging, vascular tissue regeneration, and nerve tissue regeneration indicates the potential use of MgO in these areas as well. Although this preliminary data does little other than to show the ability of MgO to self-set these polymers, this is a promising area of future research, albeit not related to orthopedic engineering.

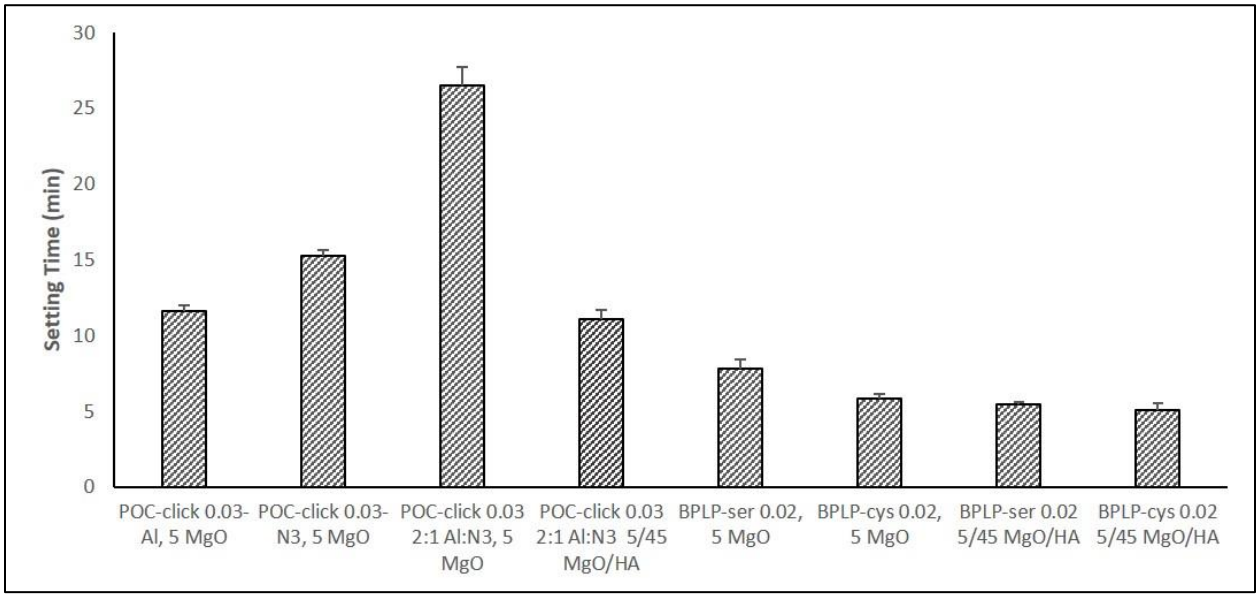

Figure 20: Setting times for other citrate-based polymers. Setting times were similar to setting times at the same conditions for POC, indicating a similar mechanism of setting. Ability of MgO to set these other citrate-based polymers indicates potential applications in areas of biomaterial research other than orthopedic biomaterials.

Chapter 4

Discussion

We proposed that MgO could act as a setting agent for POC/HA composites, improving the mechanical properties, enhancing mineralization, pH response, and degradation rate, and most importantly, providing a way to manufacture the material through previously unattainable techniques such as injection molding and 3D printing. In this work we have confirmed these characteristics of MgO doped POC/HA, illustrating the high potential for this novel material to be used in orthopedic engineering.

In exploring the self-setting ability of POC-MgO materials, it is abundantly clear that there are some factors on which the setting time is highly dependent on; these major factors appear to be temperature, POC prepolymer solution concentration, MgO concentration, POC monomer ratio, and, to some extent, the inclusion of HA in the material. By modulating these factors, the setting time of the material can be adjusted from over 300 minutes to less than 2 minutes. The most significant factor in changing the setting time was the temperature, with temperatures at and above 75^{o}C showing setting times of less than 5 minutes in almost all material formulations. As raw data, the setting time data can be difficult to understand comprehensively; thus, the processing of the data by factor analysis was an important step for better interpreting the trends in setting time. By developing a factor analysis model for the setting time as a function of four different variables (temperature, monomer ratio, POC concentration, MgO concentration) we can now computationally predict setting time for any combination of these factors. In verifying the accuracy of this predictive model, we show that at 37^{o}C and 75^{o}C the model is very accurate to the experimentally measured setting time (Fig. 23). At lower temperature, the predictive model is less accurate, with a statistically different predicted setting time than the measured value. This inaccuracy is most likely due to the high variability in the measurement of the data at room temperature, reducing the accuracy of the computational model. Although at room temperature the model lacks accuracy, at higher temperatures it is very accurate, providing a valuable tool for processing the material

and for translating from the small-scale research setting to a more industrially scaled setting geared towards producing composites for clinical applications.

Mechanical testing data shows that, in addition to providing a self-setting mechanism for citrate polymers, MgO can also significantly improve the mechanical properties of POC/HA by both increasing the peak compressive stress and by increasing the Young's modulus. At 5wt% MgO, 55wt% HA (POC(50)-MgO(5)HA(55)), cylinders showed a significant improvement over the non-thermally crosslinked POC-HA control in terms of modulus, but still lacked high compressive stress. For all three mold times (1 hr, 1d, 3d), and for both thermally and non-thermally crosslinked, the MgO containing composites shows peak stresses around 25-30 MPa. When compared to the thermally crosslinked POC-HA control (23 MPa), these cylinders did not see an improvement. The compressive modulus was significantly improved versus the POC-HA control, with values reaching above 1 GPa, compared to the 0.1-0.2 GPa modulus of the control. To better balance the added brittleness of the MgO in the composite, the MgO amount was reduced to 2.5wt% and the new system, POC(50)-MgO(2.5)HA(57.5) was tested. In this case, the compressive peak stress was much higher, with values reaching about 50 MPa. This was again a significant improvement on both the previous iteration of MgO containing composites, and the MgO free POC-HA control. Although the peak stress was much improved, by reducing the amount of MgO in the system, the modulus was also slightly decreased to about 0.9 MPa. This was still higher than the control, and closer to the goal of reaching the modulus of natural bone. From this initial data, the 1-day mold time was chosen as the only mold time to use for future tests, and the 3d 80^{o}C, 3d 120^{o}C vacuum crosslinking condition was chosen as it displayed the best mechanical properties. To again counter the brittleness of the 60wt% ceramic composites, the total ceramic amount was decreased to 50wt% and MgO was doped at 1wt%, 2.5wt%, and 5wt%. The reduction of total ceramic amount helped to significantly increase the peak stress of the material, reaching over 200 MPa in the case of POC-MgO(1)HA(49) and POC-MgO(2.5)HA(47.5) at the crosslinking condition of 1dm, 3d 80^{o}C, 3d 120^{o}C vacuum. These two formulations showed the best mechanics of all the POC-MgO/HA compositions,

almost doubling the peak stress of the control composite, and maintaining a significantly improved Young's modulus. Improving the mechanical properties of orthopedic biomaterials is an important hurdle to engineering materials which are clinically available for load bearing applications. Current materials are confined to non-loadbearing areas of bone regeneration due to low peak stress and modulus; the results seen with MgO doped POC/HA indicated that this type of material may reach the needed mechanical properties for loadbearing applications in the future, indicating a major step forward in orthopedic biomaterials.

Demonstrating easier fabrication via injection molding was a major goal of this project. Previous attempts to injection mold POC/HA have shown that this fabrication technique is near impossible with the material. However, with the self-setting ability of MgO in POC/HA composites, injection molding is now not only possible, but incredibly easy, practical, and accurate. Additionally, translating complex physiological geometries directly to the material is now quick, easy, and accurate, indicating the customizability of the material for clinical applications. In this project, the coronoid process and temporomandibular joint of the mandible were extracted from an x-ray of a human skull using MIMICS and a CAD model of an injection mold was created and 3D printed (Fig. 10). POC(50)-MgO(2.5)HA(57.5) was then injected into the mold and set for 24 hours. After setting, the material was removed from the mold and was shown to have retained the desired geometry with high accuracy. The material also retained the resolution of the 3D printed filaments in its surface, indicating a strong potential for purposeful surface modification with micro or nanoarchitecture to better improve cell attachment and proliferation. The resolution of the printer used was 200um, and this was easily retained by the material in the injection molding process. A second, higher resolution print of the mold illustrates the ability to create a more finely detailed composite. The ability to injection mold other important geometries, including screws, porous scaffolds, and micro-ridged plates was also easily demonstrated. Microridges on the surface of a plate were retained with high accuracy at a scale of less than 100um, indicating a potential for even smaller surface architecture designed to encourage cell attachment and growth. The improved ease

of fabrication with MgO allows for the fabrication of unique geometries which are not possible with previously used POC/HA; without MgO, POC/HA screws or complex geometries must be machined out of blocks of the material, increasing the waste and decreasing the overall efficiency of the process. For these materials to be viable on an industrial scale, developing more efficient pathways of fabrication is an important area; doping POC/HA with MgO allows for new ways of creating complex geometries, a definitive improvement in this area.

Accelerated degradation of POC-MgO/HA composites showed a similar degradation curve shape to POC/HA control composites, with a slightly increased degradation rate at later time points. By day 10, all three MgO containing composites (1/49, 2.5/47.5, and 5/45) showed a slightly higher rate of degradation, with almost 90% of the original composite mass degraded by day 14. Because this was an accelerated degradation test (sped up by using a low concentration NaOH solution) the degradation rates are only relative to one another, not to the true degradation time *in vivo.* Despite this, the results indicate the degradation of MgO doped POC/HA composites is not different enough from the degradation of non MgO containing composites to preclude their use in the body. In fact, a slightly increased degradation rate in the MgO doped POC/HA composites may improve the tissue ingrowth *in vivo.* A major consideration in degradable biomaterials is tuning the rate of degradation of the material to the rate of cell ingrowth and regeneration of the desired tissue. By modulating the amount of MgO in the system, the degradation rate may see a tunable nature in much the same way as the tuning of the setting time with MgO. The customizability of MgO doped POC/HA composites is an added benefit of incorporating MgO that is not seen with POC/HA.

The pH response of PBS solution to MgO doped POC/HA composites was shown to be a slight improvement on POC/HA control composites by buffering the pH at 7.4. Because POC contains carboxylic acid side chain groups, the polymer is slightly acidic; this acidity is clear in the first day of the pH testing for the control group. However, in the case of the 1/49 and 2.5/47.5 MgO doped composites, the pH was maintained at almost exactly the same level as in normal PBS (7.4). The 5/45 POC-MgO/HA

composite showed an increase in pH, likely due to the basic nature of Mg/carboxyl bonds and remaining MgO in the composite matrix. By day 10, all groups had returned to the same level, slightly above the initial 7.4 pH of the PBS. These results indicate that while the 5/45 MgO group may be too basic for use, the 1/49 and 2.5/47.5 showed an improvement in the ability of the material to maintain a physiological pH.

The swelling response of MgO-doped POC/HA composites showed again the relatively unchanged response in the 1/49 and 2.5/47.5 groups, and a slight decrease in applicability of the material in the 5/45 group. There was a slight increase in swelling between POC/HA controls and the 1/49 and 2.5/47.5 groups, however the 5/45 group showed a much higher swelling ratio which then decreased significantly over time. This decrease can most likely be attributed to the faster degradation of the 5/45 material. The high initial swelling at days 1-7 for POC-MgO/HA 5/45 suggests, as with the pH data, that this formulation may not be ideal for biomaterial use. However, in the case of the lower MgO concentration formulations (1wt% and 2.5wt%), the slight increase in swelling is not likely to pose a problem for implantation.

As with any biomaterial, the interaction between cells and the material must be examined for cytotoxicity and biocompatibility. The 24-hour cytotoxicity of MgO doped POC/HA composites was shown to be comparable to that of PLGA and POC/HA controls. As was expected, increasing the MgO amount in the composite caused a decrease in the cell viability, however even at POC-MgO(5)HA(45), the cell viability was still above 75% and comparable to the POC/HA control. Increasing MgO amount above 5wt% may cause a significant decrease in cell viability, but these higher levels of MgO are undesirable for other reasons (swelling, degradation, etc.). Although more work in the future, specifically with a bone cell line or hMSCs, would give a better understanding of the role MgO plays in cell growth, this initial data suggests that with lower levels of MgO, cytotoxic effects are minimal.

FTIR spectroscopy of the various MgO doped materials shows the mechanism of chemical crosslinking of MgO into the polymer matrix. Magnesium citrate shows a similar peak to that of POC-

MgO in the 400 cm^{-1} range, but there also exist clear peaks for the $–COO^-$ groups of the magnesium citrate tribasic, indicating that both MgO and magnesium ions exist in the composite. Because the MgO used was ~50um particle size, it is likely that these particles may react on the surface with the citrate carboxyl groups, but that there remains some unreacted MgO within the particles. It is also possible that the –COO- groups are saturated at low levels of MgO, which would explain why the size of these peaks in POC-MgO(15) are not significantly larger than in POC-MgO(5). This supports the theory that magnesium oxide has some mechanism of binding with citrate in the polymer, resulting in the setting that is observed. Although the preliminary FTIR data does support the hypothesis that the MgO binding mechanism is chemically resulting in both MgO and magnesium ions, more testing should be done to better determine exactly what this mechanism is. UV-vis spectroscopy could be used to determine the lower range of frequency (<400 cm^{-1}).

The mineralization of inorganic crystals on the surface of MgO doped composites was significantly different in morphology than the mineralization on the surface of POC/HA control composites. The characteristic cube shaped mineral deposition seen in all three MgO containing composites could possibly be attributed to magnesium cations and/or MgO leaching from the surface of the composite and then redepositing in cubic crystals. This early magnesium deposition likely alters the morphology of the crystals that are deposited through days 3-7, and results in the unique porous honey comb/strand morphology seen by day 7. It's possible that the porous platelets and thread growth are a different species of phosphate mineral, either in the form of Ca/Mg phosphate or a magnesium phosphate. Fig. 21 shows a proposed mechanism for the mineralization on MgO doped POC/HA composites. This type of mineralization pattern could provide an environment which is very conducive to cell growth and osseous tissue generation. The honeycomb shape of the mineral deposits is similar in structure to that of decellularized bone matrix, and significant recent research has examined the role that microfibers play in cell attachment and growth. If this type of mineralization could be controlled and better understood, it

may provide a massive improvement on the amorphous, spherical mineralization seen in POC/HA controls.

In addition to characterizing the ability of POC-MgO/HA composites to act as a potential orthopedic biomaterial, it was also important to demonstrate the broader impact of MgO as a self-setting doping agent in other citrate-based polymers. The citrate-based polymer family includes several other important biocompatible polymers with applications ranging from neurological tissue engineering to vascular graft repair. Additionally, many citrate-based polymers offer fluorescent character which can be used for a variety of applications, including bio sensing and imaging. MgO was combined with several of these polymers, including POC-click, BPLP, and CUPE to develop a preliminary understanding of how MgO could be applied in other areas of citrate biomaterial development. In all of the polymer combinations attempted, MgO was able to self-set the material in a comparable time to that of the original POC-MgO formulations (Fig. 20). Additionally, when MgO doped into CUPE/HA composites, the mechanical properties of the material were similar to POC-MgO/HA composites (Fig. 24, Appendix B).

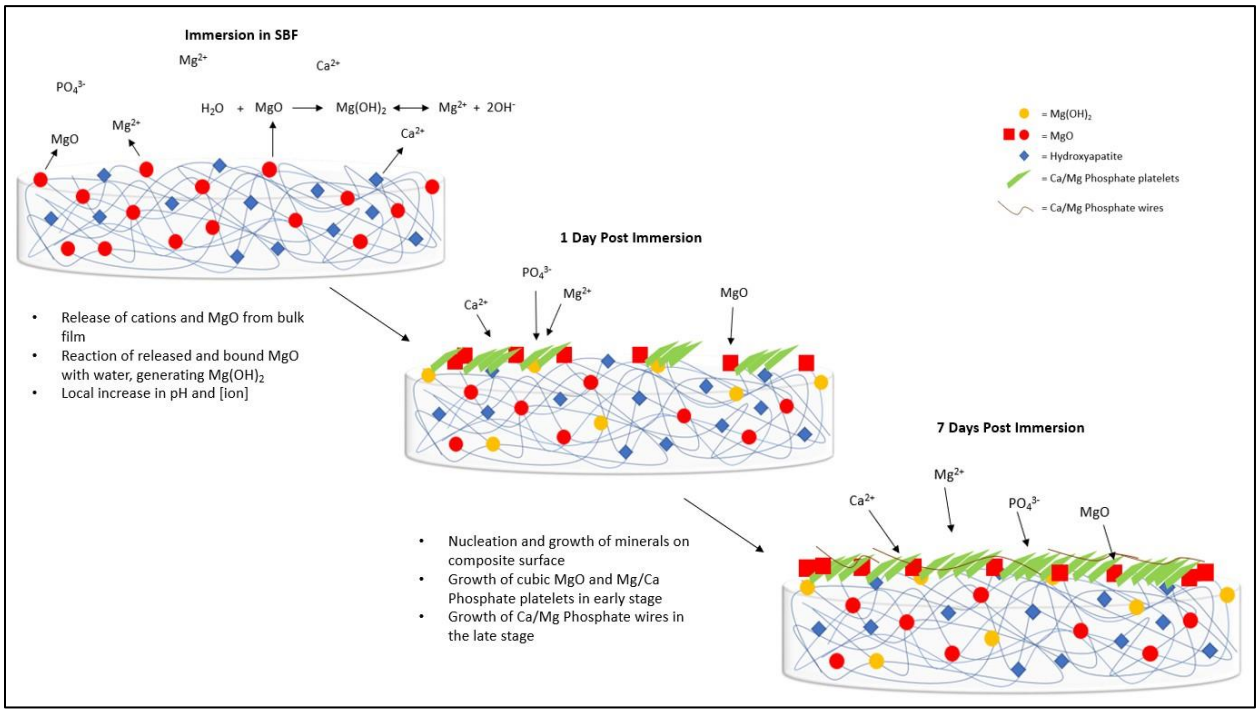

Figure 21: Proposed mechanism for mineralization on MgO doped POC/HA. MgO is released from the material soon after being placed in SBF and is then redeposited on the surface of the composite in the form of cubic crystals. Ca/Mg phosphate nucleates and grows in wire morphology and then later as smaller porous platelets.

This is an important confirmation of the universal ability of MgO to set citrate-based polymers, indicating broader applications than just orthopedic biomaterials for MgO doping.

In summary, this project has shown great potential for MgO doped POC/HA composites, and for the expansion of MgO use in other areas of citrate-based biomaterials. In addition to developing a quantitative predictive setting time model through our understanding of the factors involved in setting time, we have characterized the basic mechanical properties of the material and shown a significant improvement in the peak stress and compressive modulus of the material. Additionally, we have shown an improved ease of fabrication of the material by injection molding with little extra time or effort; this method of fabrication was previously impossible with POC/HA, which required the machining of blocks of the material to develop complex geometries. Improving the fabrication methods of the material is an important step for moving from research to industry and scaling the manufacturing process. With the ability to rapidly self-set and maintain shape and specific geometry, the MgO doped materials allow for quick injection molding, which could allow clinicians to move quickly from a scan of a defect or injury, to a solid, 3D scaffold which can be implanted immediately. We have also demonstrated that the pH, swelling, degradation, and cytotoxicity of MgO doped materials either maintain or improve the properties of POC/HA. Additionally, we showed the unique ability of MgO doped POC/HA to precipitate cubic, porous, and strand morphology minerals onto the surface of the material, indicating an interesting area of further exploration with respect to cell attachment and growth. Finally, preliminary exploration of MgO doping of other citrate-based polymers showed that MgO has a so far universal ability to set polymers synthesized from citric acid. These results indicate a potential for MgO doping in other areas of citrate biomaterial development, including applications in bio imaging and vascular repair.

Chapter 5

Conclusion

In this thesis we have demonstrated the use of magnesium oxide as a self-setting agent in citrate-based polymer composites for orthopedic applications. By modulating the composition of POC-MgO materials, the setting time can be tuned to the specific need for fabrication of more complicated scaffolds. From this raw setting time data, a factor analysis setting model was developed to predict the setting time of untested compositions, providing an important tool for scaling material fabrication, and translating it to other fabrication techniques reliant on self-setting. Simple and complex mold geometries, porous scaffolds, screws, and micro-ridged plates of POC-MgO/HA were all fabricated through injection molding, a technique previously incompatible with POC/HA materials. Additionally, magnesium oxide doped composites showed improved mechanical strength, with peak compressive stress almost double that of POC/HA control composites, and Young's moduli much closer to that of natural cortical bone. Degradation studies of the magnesium containing composites showed a slightly accelerated degradation over POC/HA control composites, and cell proliferation testing showed a comparable viability to that of POC/HA and PLGA controls. Swelling and pH testing confirmed that lower concentration MgO doped composites would be suitable for physiological use. Mineralization on MgO doped composites showed unique morphology which may improve the bioactivity of the material. Physical characterization of composite films carried out via FTIR illustrated that magnesium oxide plays a chemical role in the setting of citrate polymers by interacting with carboxyl groups in the polymer. In addition to testing with POC polymer only, magnesium oxide's self-setting ability was tested with a range of other citrate-based polymers including BPLP, CUPE, and POC-click. Magnesium oxide was a viable setting agent in all tested citrate polymers, indicating the applicability of the setting mechanism in areas other than bone

substitute materials. The results of this work show that magnesium oxide is a promising and novel doping component for both orthopedic POC/HA composites, and citrate-based materials in general.

Appendix A

Supplemental Setting Time Model

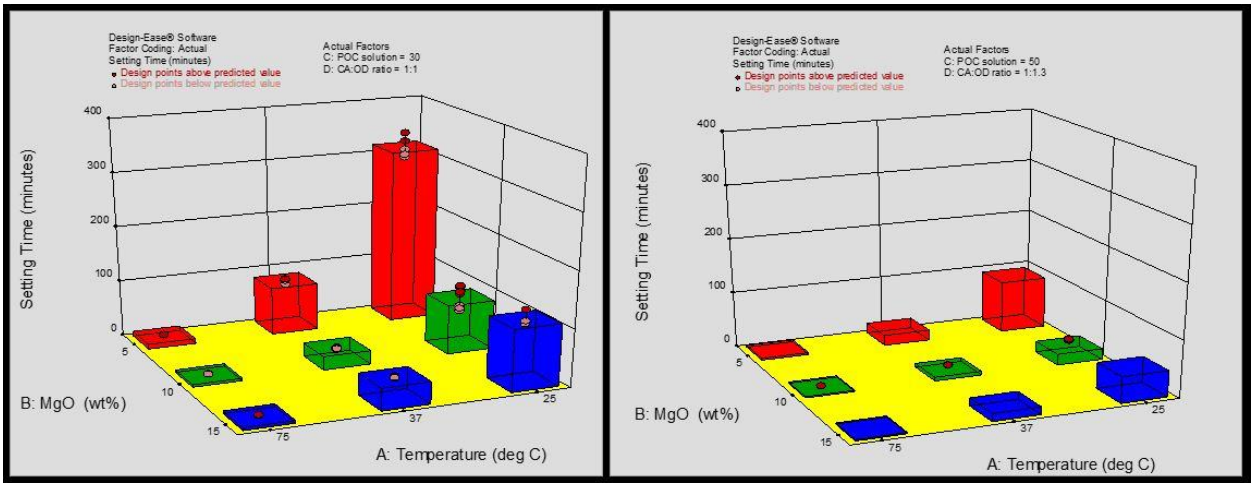

Figure 22: Design-Ease predictive setting times for untested MgO doped formulation. Red dots are experimentally measured setting times while bar height is model predicted setting time.

Table 4: ANOVA Coefficients for Factor Analysis Model

Source	Sum of Squares	df	Mean Square	F Value	p-value Prob > F	
Model	962349.7	38	25324.99	342.4642	7.7E-207	*significant*
A-Temperature	445566.3	2	222783.1	3012.647	7.8E-186	
B-MgO	75836.3	2	37918.15	512.7587	7.69E-93	
C-POC solution	73191.82	2	36595.91	494.8784	3.4E-91	
D-CA:OD ratio	83777.51	4	20944.38	283.2262	1.76E-95	
AB	74442.77	4	18610.69	251.6683	6.02E-90	
AC	63389.42	4	15847.36	214.3003	1.22E-82	
AD	80516.04	8	10064.5	136.1001	2.7E-90	
BC	42022.69	4	10505.67	142.0659	2.8E-65	
ABC	38666.69	8	4833.336	65.36012	7.05E-59	
Residual	20040.26	271	73.9493			
Lack of Fit	11626.89	20	581.3445	17.34352	1.17E-36	*significant*
Pure Error	8413.371	251	33.51941			
Cor Total	982390	309				

Table 5: Setting Time Factor Coefficients

Term	Coefficient Estimate	df	Standard Error	95% CI Low	95% CI High
Intercept	51.70337	1	0.984489	49.76515	53.64159
A[1]	-16.5063	1	0.399946	-17.2937	-15.7189
A[2]	8.483577	1	0.320349	7.852887	9.114266
B[1]	-18.7156	1	0.906454	-20.5001	-16.931
B[2]	11.24086	1	0.482547	10.29084	12.19088
C[1]	-25.0032	1	0.776361	-26.5317	-23.4748
C[2]	5.291338	1	0.452519	4.400438	6.182238
D[1]	-4.97935	1	1.062879	-7.0719	-2.8868
D[2]	41.0808	1	1.178143	38.76132	43.40027
D[3]	-2.64796	1	1.178143	-4.96743	-0.32848
D[4]	-25.2869	1	1.601001	-28.4389	-22.1349
A[1]B[1]	6.310562	1	0.368607	5.584864	7.036259
A[2]B[1]	-3.74827	1	0.294667	-4.3284	-3.16814
A[1]B[2]	-3.73786	1	0.196221	-4.12417	-3.35155
A[2]B[2]	1.865239	1	0.15687	1.556401	2.174077
A[1]C[1]	7.942484	1	0.315644	7.321057	8.56391
A[2]C[1]	-3.52264	1	0.252426	-4.01961	-3.02568
A[1]C[2]	-1.67863	1	0.184016	-2.04091	-1.31635
A[2]C[2]	0.710825	1	0.147104	0.421214	1.000436
A[1]D[1]	1.596785	1	0.431911	0.746457	2.447113
A[2]D[1]	-0.57987	1	0.345762	-1.26059	0.100846
A[1]D[2]	-13.4793	1	0.478639	-14.4217	-12.537
A[2]D[2]	6.705868	1	0.383347	5.951152	7.460584
A[1]D[3]	0.655255	1	0.478639	-0.28707	1.597578
A[2]D[3]	0.15881	1	0.383347	-0.59591	0.913526
A[1]D[4]	8.479436	1	0.646291	7.207047	9.751825
A[2]D[4]	-4.85161	1	0.52422	-5.88367	-3.81955
B[1]C[1]	16.9905	1	1.110175	14.80484	19.17616
B[2]C[1]	-5.80928	1	0.438072	-6.67173	-4.94682
B[1]C[2]	-7.29961	1	0.64096	-8.5615	-6.03772
B[2]C[2]	1.508273	1	0.260443	0.995525	2.021021
A[1]B[1]C[1]	-5.67867	1	0.45145	-6.56746	-4.78987
A[2]B[1]C[1]	2.8636	1	0.360892	2.15309	3.574109
A[1]B[2]C[1]	1.825483	1	0.178033	1.47498	2.175987
A[2]B[2]C[1]	-0.67567	1	0.142494	-0.9562	-0.39513
A[1]B[1]C[2]	2.523208	1	0.260645	2.010062	3.036353
A[2]B[1]C[2]	-1.46848	1	0.208361	-1.87869	-1.05826
A[1]B[2]C[2]	-0.49371	1	0.105908	-0.70222	-0.2852
A[2]B[2]C[2]	0.253444	1	0.084664	0.086761	0.420127

Equation 3: Setting Time Predictive Equation

Setting Time	=
51.70337281	
-16.50629531	* A[1]
8.483576525	* A[2]
-18.71555556	* B[1]
11.24086294	* B[2]
-25.00322483	* C[1]
5.291338058	* C[2]
-4.979346863	* D[1]
41.08079753	* D[2]
-2.647958028	* D[3]
-25.28692794	* D[4]
6.310561535	* A[1]B[1]
-3.748268102	* A[2]B[1]
-3.737856166	* A[1]B[2]
1.865239012	* A[2]B[2]
7.942483797	* A[1]C[1]
-3.522643743	* A[2]C[1]
-1.678632757	* A[1]C[2]
0.710825026	* A[2]C[2]
1.596784979	* A[1]D[1]
-0.579874245	* A[2]D[1]
-13.47933396	* A[1]D[2]
6.705868232	* A[2]D[2]
0.655255098	* A[1]D[3]
0.158809523	* A[2]D[3]
8.479435997	* A[1]D[4]
-4.851610762	* A[2]D[4]
16.9905	* B[1]C[1]
-5.809275167	* B[2]C[1]
-7.299611111	* B[1]C[2]
1.508273053	* B[2]C[2]
-5.678665851	* A[1]B[1]C[1]
2.863599804	* A[2]B[1]C[1]
1.825483424	* A[1]B[2]C[1]
-0.67566839	* A[2]B[2]C[1]
2.523207708	* A[1]B[1]C[2]
-1.468476517	* A[2]B[1]C[2]
-0.493710633	* A[1]B[2]C[2]
0.253444055	* A[2]B[2]C[2]

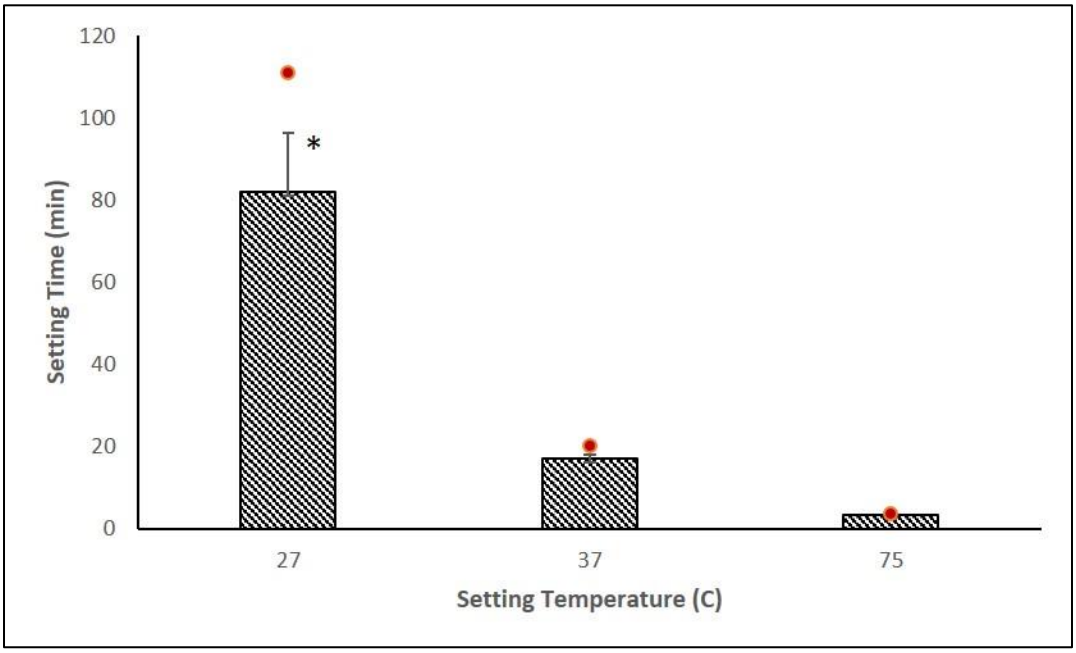

Figure 23: POC-MgO 1.3:1 50wt% POC, 5wt% MgO setting time. Red dot is model predicted value, bar height it measured value. (* indicates $p<0.05$)

Appendix B

Supplemental Mechanical Data

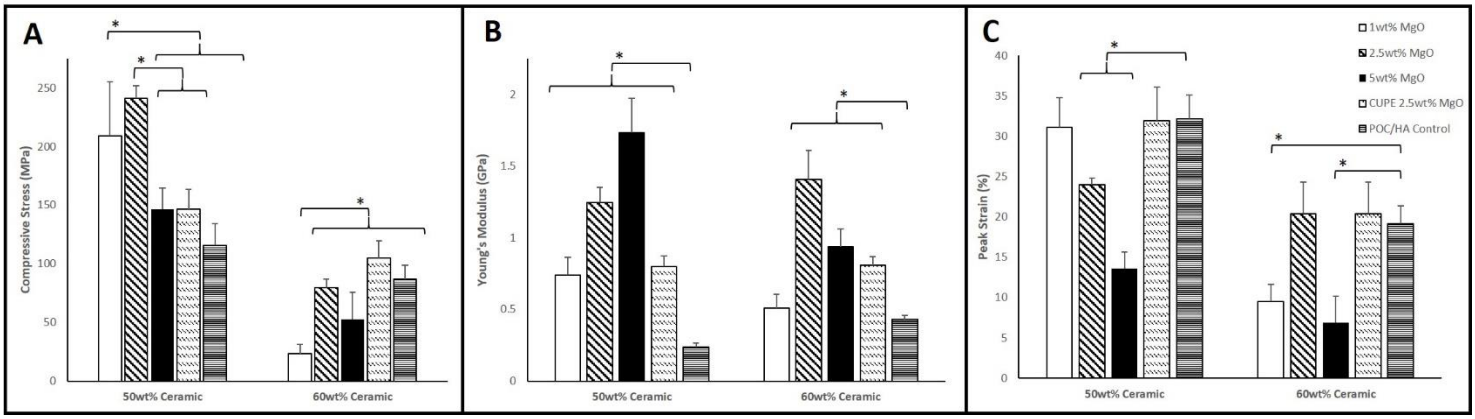

Figure 24: CUPE-MgO/HA mechanical properties at 3d 80ºC, 3d 120ºC vacuum. Subfigure A shows peak stress, subfigure B shows Young's modulus, and subfigure C shows peak strain. CUPE-MgO/HA composites show similar properties to POC-MgO/HA composites, indicating the potential for the use of MgO in other citrate-based polymers while maintaining mechanical properties. (* indicates $p<0.05$)

BIBLIOGRAPHY

1. Laurencin C, Khan Y, El-Amin SF. Bone graft substitutes. *Expert Rev Med Devices*. 2006;3(1):49-57. doi:10.1586/17434440.3.1.49.

2. Peltier LF, Bickel EY, Lillo R, Thein MS. The use of plaster of paris to fill defects in bone. *Ann Surg*. 1957;146(1):61-69.

3. Fukase Y, Eanes ED, Takagp S, Chow LC, Brown WE. Setting Reactions and Compressive Strengths of Calcium Phosphate Cements. *J Dent Res*. 1990;69(12):1852-1856. doi:10.1177/00220345900690121201.

4. Schmitz J, Hollinger J, Milam S. Reconstruction of bone using calcium phosphate bone cements: A critical review. *J Oral Maxillofac Surg*. 1999;57(9):1122-1126. doi:10.1016/S0278-2391(99)90338-5.

5. Ambard AJ, Mueninghoff L. Calcium Phosphate Cement: Review of Mechanical and Biological Properties. *J Prosthodont*. 2006;15(5):321-328. doi:10.1111/j.1532-849X.2006.00129.x.

6. Luca L, Rougemont AL, Walpoth BH, et al. Injectable rhBMP-2-loaded chitosan hydrogel composite: Osteoinduction at ectopic site and in segmental long bone defect. *J Biomed Mater Res - Part A*. 2011;96 A(1):66-74. doi:10.1002/jbm.a.32957.

7. Kim HK, Shim WS, Ph D, et al. Injectable In Situ – Forming pH = Thermo-Sensitive Hydrogel for Bone Tissue Engineering. *Tissue Eng Part A*. 2009;15(4).

8. Dyondi D, Webster TJ, Banerjee R. A nanoparticulate injectable hydrogel as a tissue engineering scaffold for multiple growth factor delivery for bone regeneration. *Int J Nanomedicine*. 2012;8:47-59. doi:10.2147/IJN.S37953.

9. Martínez-Sanz E, Ossipov DA, Hilborn J, Larsson S, Jonsson KB, Varghese OP. Bone reservoir: Injectable hyaluronic acid hydrogel for minimal invasive bone augmentation. *J Control Release*. 2011;152(2):232-240. doi:10.1016/j.jconrel.2011.02.003.

10. Zhao L, Weir MD, Xu HHK. An injectable calcium phosphate-alginate hydrogel-umbilical cord mesenchymal stem cell paste for bone tissue engineering. *Biomaterials*. 2010;31(25):6502-6510. doi:10.1016/j.biomaterials.2010.05.017.

11. Akkineni AR, Luo Y, Schumacher M, Nies B, Lode A, Gelinsky M. 3D plotting of growth factor loaded calcium phosphate cement scaffolds. *Acta Biomater*. 2015;27:264-274. doi:10.1016/j.actbio.2015.08.036.

12. Ahlfeld T, Akkineni AR, Förster Y, et al. Design and Fabrication of Complex Scaffolds for Bone Defect Healing: Combined 3D Plotting of a Calcium Phosphate Cement and a Growth Factor-Loaded Hydrogel. *Ann Biomed Eng*. 2017;45(1):224-236. doi:10.1007/s10439-016-1685-4.

13. Pastorino D, Canal C, Ginebra MP. Drug delivery from injectable calcium phosphate foams by tailoring the macroporosity-drug interaction. *Acta Biomater*. 2015;12(1):250-259. doi:10.1016/j.actbio.2014.10.031.

14. Lopez-Heredia MA, Bernard Kamphuis GJ, Thüne PC, Cumhur Öner F, Jansen JA, Frank Walboomers X. An injectable calcium phosphate cement for the local delivery of paclitaxel to bone. *Biomaterials*. 2011;32(23):5411-5416. doi:10.1016/j.biomaterials.2011.04.010.

15. Mostafa NY, Zaki ZI. Injectable Bone Cement Based on Calcium Silicate and Calcium Phosphate. *Int J Chem Sci*. 2015;13(1):80-96.

16. Zhang Y, Wu Z, Shu Y, Wang F, Cao W, Li W. A novel bioactive vaterite-containing tricalcium silicate bone cement by self hydration synthesis and its biological properties. *Mater Sci Eng C*.

2017;79:23-29. doi:10.1016/j.msec.2017.05.025.

17. Han Y, Zeng Q, Li H, Chang J. The calcium silicate/alginate composite: Preparation and evaluation of its behavior as bioactive injectable hydrogels. *Acta Biomater*. 2013;9(11):9107-9117. doi:10.1016/j.actbio.2013.06.022.

18. Khoshakhlagh P, Rabiee SM, Kiaee G, et al. Development and characterization of a bioglass/chitosan composite as an injectable bone substitute. *Carbohydr Polym*. 2017;157:1261-1271. doi:10.1016/j.carbpol.2016.11.003.

19. Rosato D V. *Injection Molding Handbook*.; 2000.

20. Abu Bakar MS, Chenag P, Khor KA. Mechanical properties of injection molded hydroxyapatite-polyetheretherketone biocomposites. *Compos Sci Technol*. 2003;63(3-4):421-425. doi:10.1016/S0266-3538(02)00230-0.

21. Kramschuster A, Turng L-S. An injection molding process for manufacturing highly porous and interconnected biodegradable polymer matrices for use as tissue engineering scaffolds. *J Biomed Mater Res Part B Appl Biomater*. 2009;9999B:NA-NA. doi:10.1002/jbm.b.31523.

22. Gomes ME, Ribeiro AS, Malafaya PB, Reis RL, Cunha AM. A new approach based on injection moulding to produce biodegradable starch-based polymeric scaffolds: Morphology, mechanical and degradation behaviour. *Biomaterials*. 2001. doi:10.1016/S0142-9612(00)00211-8.

23. Wu L, Jing D, Ding J. A “room-temperature” injection molding/particulate leaching approach for fabrication of biodegradable three-dimensional porous scaffolds. *Biomaterials*. 2006;27(2):185-191. doi:10.1016/j.biomaterials.2005.05.105.

24. Inzana JA, Olvera D, Fuller SM, et al. 3D printing of composite calcium phosphate and collagen

scaffolds for bone regeneration. *Biomaterials*. 2014;35(13):4026-4034. doi:10.1016/j.biomaterials.2014.01.064.

25. Cox S, Thornby J, Gibbons G, Williams M, Mallick K. 3D printing of porous hydroxyapatite scaffolds intended for use in bone tissue engineering applications. *Mater Sci Eng C*. 2015;47:237-247. doi:10.1016/J.MSEC.2014.11.024.

26. Lode A, Meissner K, Luo Y, et al. Fabrication of porous scaffolds by three-dimensional plotting of a pasty calcium phosphate bone cement under mild conditions. *J Tissue Eng Regen Med*. 2014;8(9):682-693. doi:10.1002/term.1563.

27. Tran R, Zhang Y, Gyawali D, Yang J. Recent Developments on Citric Acid Derived Biodegradable Elastomers. *Recent Patents Biomed Eng*. 2009;2(3):216-227. doi:10.2174/1874764710902030216.

28. Yang J, Webb AR, Ameer GA. Novel Citric Acid-Based Biodegradable Elastomers for Tissue Engineering. *Adv Mater*. 2004;16(6):511-516. doi:10.1002/adma.200306264.

29. Tran RT, Yang J, Ameer GA. Citrate-Based Biomaterials and Their Applications in Regenerative Engineering. *Annu Rev Mater Res*. 2015;45(1):277-310. doi:10.1146/annurev-matsci-070214-020815.

30. Hu Y-Y, Rawal A, Schmidt-Rohr K. Strongly bound citrate stabilizes the apatite nanocrystals in bone. *Proc Natl Acad Sci U S A*. 2010;107(52):22425-22429. doi:10.1073/pnas.1009219107.

31. Qiu H, Yang J, Kodali P, Koh J, Ameer GA. A citric acid-based hydroxyapatite composite for orthopedic implants. *Biomaterials*. 2006;27(34):5845-5854. doi:10.1016/j.biomaterials.2006.07.042.

32. Niinomi M. Recent metallic materials for biomedical applications. *Metall Mater Trans A*. 2002;33(3):477-486. doi:10.1007/s11661-002-0109-2.

33. Staiger M, Pietaka A, Huadmai J, Dias G. Magnesium and its alloys as orthopedic biomaterials: A review. *Biomaterials*. 2006;27(9):1728-1734. doi:10.1016/J.BIOMATERIALS.2005.10.003.

34. Zreiqat H, Howlett CR, Zannettino A, et al. Mechanisms of magnesium-stimulated adhesion of osteoblastic cells to commonly used orthopaedic implants. *J Biomed Mater Res*. 2002;62(2):175-184. doi:10.1002/jbm.10270.

35. Yamasaki Y, Yoshida Y, Okazaki M, et al. Synthesis of functionally graded MgCO3 apatite accelerating osteoblast adhesion. *J Biomed Mater Res*. 2002;62(1):99-105. doi:10.1002/jbm.10220.

36. Yamasaki Y, Yoshida Y, Okazaki M, et al. Action of FGMgCO3Ap-collagen composite in promoting bone formation. *Biomaterials*. 2003;24(27):4913-4920.

37. Witte F, Kaese V, Haferkamp H, et al. In vivo corrosion of four magnesium alloys and the associated bone response. *Biomaterials*. 2005;26(17):3557-3563. doi:10.1016/j.biomaterials.2004.09.049.

38. Tan C, Yaghoubi A, Ramesh S, et al. Sintering and mechanical properties of MgO-doped nanocrystalline hydroxyapatite. *Ceram Int*. 2013;39(8):8979-8983. doi:10.1016/J.CERAMINT.2013.04.098.

39. Banerjee S, Tarafder S, Davies N, Bandyopadhyay A, Bose S. Understanding the influence of MgO and SrO binary doping on the mechanical and biological properties of β-TCP ceramics. *Acta Biomater*. 2010;6(10):4167-4174. doi:10.1016/J.ACTBIO.2010.05.012.

40. Jia J, Zhou H, Wei J, et al. Development of magnesium calcium phosphate biocement for bone regeneration. *J R Soc Interface*. 2010;7(49):1171-1180. doi:10.1098/rsif.2009.0559.

41. Li X, Niu Y, Guo H, et al. Preparation and osteogenic properties of magnesium calcium phosphate biocement scaffolds for bone regeneration. *J Instrum*. 2013;8(7):C07010-C07010. doi:10.1088/1748-0221/8/07/C07010.

42. Liu W, Zhang J, Rethore G, et al. A novel injectable, cohesive and toughened Si-HPMC (silanized-hydroxypropyl methylcellulose) composite calcium phosphate cement for bone substitution. *Acta Biomater*. 2014;10(7):3335-3345. doi:10.1016/j.actbio.2014.03.009.

43. Zima A, Czechowska J, Siek D, Ślósarczyk A. Influence of magnesium and silver ions on rheological properties of hydroxyapatite/chitosan/calcium sulphate based bone cements. 2017. doi:10.1016/j.ceramint.2017.08.197.

44. Krajewska B. Diffusion of metal ions through gel chitosan membranes. *React Funct Polym*. 2001. doi:10.1016/S1381-5148(00)00068-7.

45. Christel T, Christ S, Barralet JE, Groll J, Gbureck U. Chelate bonding mechanism in a novel magnesium phosphate bone cement. *J Am Ceram Soc*. 2015;98(3):694-697. doi:10.1111/jace.13491.

46. Konishi T, Mizumoto M, Honda M, et al. Fabrication of novel biodegradable α-tricalcium phosphate cement set by chelating capability of inositol phosphate and its biocompatibility. *J Nanomater*. 2013. doi:10.1155/2013/864374.

Academic Vita

KEVIN RAHN

Kevin.rahn8@gmail.com

EDUCATION

Bachelor of Science, Biomedical Engineering
Schreyer Honors College
The Pennsylvania State University, University Park, PA
Graduation: May 2018

EXPERIENCE

Transformative Biomaterials and Biotechnology Lab, Penn State
Research Assistant *January 2015-May 2018*

- Investigated bioactive and biodegradable citrate-based polymers and composites for bone scaffolding
- Synthesized various pre-polymers, constructed citrate-based composites, conducted mechanical strength testing of cylindrical composites and bioadhesive films, and investigated bioactivity of composites and films
- Granted Spring 2016 CERI REU to investigate tannic acid as a bridge bioadhesive in biodegradable polymer/HA composites

Cartilage Bioengineering Laboratory, University of Delaware
Summer REU Participant *Summer 2017*

- Investigated the potential of carbon nanotube sponges in the capture and diagnoses of circulating cancer cells
- Cultured human breast cancer cell lines for extracellular matrix synthesis rate characterization
- Presented findings at Undergraduate research symposium at the University of Delaware

Mount Nittany Medical Center
Volunteer *Fall 2012-Fall 2013*

- Responsible for timely delivery of necessary medical equipment throughout hospital
- Fostered efficient communication with nurses and medical staff about patient discharge

SKILLS

Proficient in Matlab, COMSOL, and SolidWorks
Basic Knowledge of speaking, reading, and writing French

HONORS & AWARDS

Dean's List: Fall 2014, Spring 2015, Fall 2015, Fall 2016, Spring 2016, Fall 2016, Spring 2017, Fall 2017, Spring 2018
Recipient, Penn State Engineering Design Showcase "Most Innovative Design" (2015)
Schreyer Honor's College Scholarship (2014-2018)